TU Delft

Delft University of Technology

Delamination fatigue growth in polymer-matrix fibre composites
A methodology for determining the design and lifing allowables

Yao, Liaojun; Alderliesten, R. C.; Jones, R.; Kinloch, A. J.

DOI
10.1016/j.compstruct.2018.04.069

Publication date
2018

Document Version
Accepted author manuscript

Published in
Composite Structures

Citation (APA)
Yao, L., Alderliesten, R. C., Jones, R., & Kinloch, A. J. (2018). Delamination fatigue growth in polymer-matrix fibre composites: A methodology for determining the design and lifing allowables. *Composite Structures*, *196*, 8-20. https://doi.org/10.1016/j.compstruct.2018.04.069

Important note
To cite this publication, please use the final published version (if applicable).
Please check the document version above.

Copyright
Other than for strictly personal use, it is not permitted to download, forward or distribute the text or part of it, without the consent of the author(s) and/or copyright holder(s), unless the work is under an open content license such as Creative Commons.

Takedown policy
Please contact us and provide details if you believe this document breaches copyrights.
We will remove access to the work immediately and investigate your claim.

This work is downloaded from Delft University of Technology.
For technical reasons the number of authors shown on this cover page is limited to a maximum of 10.

© 2018 Manuscript version made available under CC-BY-NC-ND 4.0 license
https://creativecommons.org/licenses/by-nc-nd/4.0/

Delamination Fatigue Growth in Polymer-Matrix Fibre Composites: A Methodology for Determining the Design and Lifing Allowables

Liaojun Yao[1] , R.C. Alderliesten[1], R. Jones[2], A. J. Kinloch[3]

[1] Structural Integrity and Composites Group, Faculty of Aerospace Engineering, Delft University of Technology, The Netherlands.
[2] Centre of Expertise for Structural Mechanics, Department of Mechanical and Aerospace Engineering, Monash University, Clayton, Victoria, 3800, Australia.
[3] Department of Mechanical Engineering, Imperial College London, Exhibition Road, London SW7 2AZ, UK.

Corresponding authors: rhys.jones@monash.edu; a.kinloch@imperial.ac.uk

Abstract:

The introduction, originally in 2009, by the FAA of a 'slow growth' approach to the certification of polymer-matrix fibre composites has focused attention on the experimental data and the analytical tools needed to assess the growth of delaminations under cyclic-fatigue loads. Of direct relevance is the fact that fatigue tests on aircraft composite components and structures reveal that no, or only little, retardation of the fatigue crack growth (FCG) rate occurs as delamination/impact damage grows. Therefore, of course, the FCG data that are ascertained in laboratory tests, and then employed as a material-allowable property to design and life the structure, as well as for the development, characterisation and comparison of composite materials, must also exhibit no, or only minimal, retardation. Now, in laboratory tests the double-cantilever beam (DCB) test, using a typical carbon-fibre reinforced-plastic (CFRP) aerospace composite, is usually employed to obtain fracture-mechanics data under cyclic-fatigue Mode I loading. However, it is extremely difficult to perform such DCB fatigue tests without extensive fibre-bridging developing across the crack faces. This fibre-bridging leads to significant retardation of the FCG rate. Such fibre-bridging, and hence retardation of the FCG, is seen to arise even for the smallest values of the pre-crack extension length, a_p - a_0, that are typically employed. The results from the DCB tests also invariably exhibit a relatively large degree of inherent scatter. Thus, a methodology is proposed for predicting an 'upper-bound' FCG curve from the laboratory test data which is representative of a composite laminate exhibiting no, or only very little, retardation of the FCG rate under fatigue loading and which takes into account the inherent scatter. To achieve this we have employed a novel methodology, based on using a variant of the Hartman-Schijve equation, to access this 'upper-bound' FCG rate curve, which may be thought of as a material-allowable property and which is obtained using an 'A basis' statistical approach. Therefore, a conservative 'upper-bound' FCG curve may now be calculated from the DCB laboratory test data for material development, characterisation and comparative studies, and for design and lifing studies.

Keywords: composites; fatigue; fracture mechanics; delamination growth

NOMENCLATURE

a	total crack (delamination) length, measured from the loading line
a_0	length of the initial delamination in the test specimen, i.e. the length of the (thin) film used as a starter crack, measured from the loading line
a_p	length of the pre-crack (pre-delamination), measured from the loading line, in the test specimen prior to any cyclic-fatigue fracture measurements being taken
a_p-a_0	pre-crack (pre-delamination) extension length in the test specimen prior to any cyclic-fatigue fracture measurements being taken
A	a constant in the Hartman-Schijve equation
A_0	value of A when the value of (a_p-a_0) tends to zero
CDF	crack driving force
CFRP	carbon-fibre reinforced-plastic
da/dN	rate of fatigue crack growth per cycle
D	intercept in the Hartman-Schijve crack-growth equation
DCB	double-cantilever beam
F_{max}	maximum load applied during the fatigue test
F_{min}	minimum load applied during the fatigue test
FAA	Federal Aviation Administration
FCG	fatigue crack growth
FRP	fibre-reinforced plastic
G	energy release-rate
G_{app}	applied value of G
G_c	quasi-static value of the fracture energy
G_{c0}	quasi-static value of the initiation fracture energy for the onset of crack growth
G_{max}	maximum value of the applied energy release-rate in the fatigue cycle
G_{min}	minimum value of the applied energy release-rate in the fatigue cycle
G_{tip}	value of G at the tip of the delamination in the absence of fibre bridging
ΔG	range of the applied energy release-rate in the fatigue cycle, as defined below
ΔG	$= G_{max} - G_{min}$
$\Delta\sqrt{G}$	range of the applied energy release-rate in the fatigue cycle, as defined below
$\Delta\sqrt{G}$	$= \sqrt{G_{max}} - \sqrt{G_{min}}$
$\Delta\sqrt{G_{th}}$	the value of $\Delta\sqrt{G}$ corresponding to a FCG rate, $da/dN = 10^{-10}$ m/cycle
$\Delta\sqrt{G_{thr}}$	range of the fatigue threshold value of $\Delta\sqrt{G}$, as defined below
$\Delta\sqrt{G_{thr}}$	$= \sqrt{G_{thr.max}} - \sqrt{G_{thr.min}}$
$\sqrt{G_{thr.max}}$	threshold value of $\sqrt{G_{max}}$
$\sqrt{G_{thr.min}}$	threshold value of $\sqrt{G_{min}}$
$\Delta\sqrt{G_{thr0}}$	value of $\Delta\sqrt{G_{thr}}$ when the value of (a_p-a_0) tends to zero
K	stress-intensity factor

K_{max}	maximum value of the applied stress-intensity factor in the fatigue cycle
K_{min}	minimum value of the applied stress-intensity factor in the fatigue cycle
ΔK	range of the applied stress-intensity factor in the fatigue cycle, as defined below
ΔK	$= K_{max} - K_{min}$
n	exponent in the Hartman-Schijve crack-growth equation
N	number of fatigue cycles
R	stress ratio ($=F_{min}/F_{max}$)
R^2	the linear correlation coefficient
W	strain-energy density
I, II	subscripts indicating Mode I (opening tensile) and Mode II (in-plane shear) loads

1. INTRODUCTION

The growth of delaminations in polymer-matrix fibre composites under cyclic-fatigue loading in operational aircraft structures is an important factor which has the potential to significantly affect the service-life of the airframe. In this context it is important to note the introduction [1], originally in 2009, by the Federal Aviation Administration (FAA) of a 'slow growth' approach to the certification of such composites and the examples of delamination growth in aircraft components and structures which have been reported in the open literature, see [2,3] for more details. These aspects have focused attention on the experimental data, and the analytical tools, needed to assess the growth of such delaminations under fatigue loads. One of the most common methods employed to assess the fatigue delamination resistance of fibre-reinforced plastics (FRPs) is to use a fracture-mechanics approach [2, 4-39] to determine experimentally the dependence of the fatigue crack growth (FCG) rate upon some function related to the applied energy release-rate, G, in the fatigue cycle. Therefore, the present paper addresses the growth of delaminations in FRPs under cyclic-fatigue loading using such an approach.

Now, of direct relevance is the fact that previous studies on actual aircraft components and structures have revealed no, or only little, retardation in the (delamination) FCG rate. For example, in [2, 40-44] it has been shown that the fastest growing, i.e. lead, delaminations that arise under the cyclic-fatigue loading of aircraft components with mis-drilled holes, ply drop-offs, impact damage, manufacturing defects, etc. show no, or only very little, retardation.

Therefore, a first main requirement is that the FCG rate results that are ascertained from fracture-mechanics tests undertaken in the laboratory, and subsequently employed for certification or aircraft sustainment analyses, must also exhibit no, or only minimal, retardation. Only if this is the case may the FCG rate data obtained from such laboratory tests be reliably employed as material-allowable properties to design and life composite components and structures, as well as for the development, characterisation and comparison of composite materials. However, in fracture-mechanics tests, such as when the very commonly-used Mode I double-cantilever beam (DCB) specimen is employed, retardation of the FCG arising from fibre-bridging developing across the faces of the delamination as the fatigue crack advances is invariably observed and, as discussed in detail below, the development of such fibre-bridging cannot readily be prevented. Indeed, even if multidirectional or quasi-isotropic lay-ups, as opposed to unidirectional laminates, are employed for the DCB tests, then fibre-bridging, or even multiple-ply cracks leading to ply-bridging, generally still develop, as discussed later in the present paper.

A second main requirement for any methodology used to determine FCG rate data as a function of G, where this relationship could be considered as an accurate and valid material-allowable property, is to take into account the relatively large inherent scatter that is observed in the laboratory tests, whatever its source. It is now appreciated [2,16,19,21,24,28,32-37,39] that fibre-bridging effects may give rise, at least in part, to the relatively large scatter that is typically seen in fatigue tests on FRPs. However, there are other likely sources of such scatter [2,16,19,25,33]. These include, for example, (a) any variability in the manufacturing procedures, which can lead to variability in the composite laminate test specimens, and (b) experimental difficulties associated with accurately measuring the crack length and the relatively very low loads and displacements associated with such tests, especially as the test approaches the threshold region below which no significant FCG occurs.

From the above comments, it is therefore obviously of little use to determine an 'average' delamination growth curve from the fracture-mechanics tests undertaken in the laboratory. The same comments hold with respect to determining an accurate and valid value of the fatigue threshold, below which no significant FCG occurs. Clearly, the fracture-mechanics fatigue tests should be performed in order (a) to determine a delamination FCG curve that focuses on ensuring that the fastest possible growth curve is measured, i.e. one which is free of retardation effects, and (b) to assess quantitatively the typical scatter that is always observed with such measurements. However, the experimental data reveal that retardation effects, e.g. from fibre-bridging, and a relatively high degree of inherent scatter cannot usually be avoided. Thus, a methodology is needed for estimating an 'upper-bound curve' from the laboratory test results that (a) that encompasses all the experimental data considered by the present authors, (b) provides a conservative FCG curve which accounts for any retardation effects, and (c) accounts for the experimental scatter that is frequently seen under fatigue loading. Such an 'upper-bound' FCG curve can then employed for developing, characterising and comparing different composite materials, and for designing and lifing in-service aircraft components and structures, using a 'slow growth' approach.

The recent paper [2] proposed a novel methodology, based on using a variant of the Hartman-Schijve equation [45], to determine a valid 'upper-bound' FCG curve, which may be thought of as a material-allowable property and accounts for both fibre-bridging effects and experimental scatter. The aim of the present paper is, therefore, to investigate whether this methodology can be extended to a carbon-fibre reinforced-plastic (CFRP) composite for which a very extensive testing programme has been previously undertaken and reported [26,35-37,46].

2. THEORETICAL BACKGROUND

Due to the inhomogeneity and anisotropy of FRPs, the energy release-rate, *G*, approach, rather than the stress-intensity factor approach, is generally used to study delamination growth in such materials [47-49]. Thus, by analogy with the extensive work [50-52] of Paris and others on metals, where the range, ΔK, of the applied stress-intensity factor is invariably employed to analyse the data, at first sight the most obvious and corresponding parameter against which to plot the measured rate of FCG, *da/dN*, for FRPs is the range of the applied energy release-rate, ΔG, such that:

$$\Delta G = G_{max} - G_{min} \tag{1}$$

Here G_{max} and G_{min} are the maximum and minimum values of the applied energy release-rate in a fatigue cycle, respectively. The use of the maximum value of the energy release-rate, G_{max}, has also been quite widely employed as the parameter in the FCG plots [7]. However, recent work has revealed [2,13,27,28,30,53] that the logical extension of the Paris FCG equation for metals to delamination growth in FRPs is, in fact, to express *da/dN* as a function of $\Delta\sqrt{G}$, or $\sqrt{G_{max}}$, rather than ΔG, or G_{max}. Where $\Delta\sqrt{G}$ is given by:

$$\Delta\sqrt{G} = \sqrt{G_{max}} - \sqrt{G_{min}} \tag{2}$$

Following these ideas, and as noted above, a novel empirical methodology based on using a variant of the Hartman-Schijve equation has been proposed [2] to access the 'upper-bound' FCG rate curve, which may be thought of as a material-allowable property. The form [45] of the Hartman and Schijve equation, which is a variant of the Nasgro equation [54], in terms of $\Delta\sqrt{G}$ is [30,31]:

$$\frac{da}{dN} = D\left[\frac{\Delta\sqrt{G} - \Delta\sqrt{G_{thr}}}{\sqrt{\{1-\sqrt{G_{max}}/\sqrt{A}\}}}\right]^n \tag{3}$$

where *D*, *n* and *A* are constants. The term *A* is best interpreted as a parameter chosen so as to fit the experimentally-measured data but it has been found [2] to be very close in value to the quasi-static value of the initiation fracture energy, G_{c0}, for the onset of crack growth. The term $\Delta\sqrt{G_{thr}}$ is defined by:

$$\Delta\sqrt{G_{thr}} = \sqrt{G_{thr.max}} - \sqrt{G_{thr.min}} \tag{4}$$

and the subscript '*thr*' in Equation (3) and (4) refers to the values at threshold, below which no significant FCG occurs. (It should be noted that FRPs may undergo delamination under Mode I (opening tensile) and Mode II (in-plane shear) loading. Thus, the subscripts I and II are used to indicate the mode of loading, as appropriate.) As explained in [2,18,27,30] the values of A and $\Delta\sqrt{G_{thr}}$ are best chosen so as to ensure that Equation (3) fits the experimental data over the entire range of crack growth rates, see Appendix A. It should be noted that the term $\Delta\sqrt{G_{thr}}$ differs from $\Delta\sqrt{G_{th}}$, where $\Delta\sqrt{G_{th}}$ is the value $\Delta\sqrt{G}$ of corresponding to a crack growth rate, da/dN = 10^{-10} m/cycle. The mathematical relationship between these two terms is given in Appendix B.

Finally, it is noteworthy that the use of the strain-energy density, W, for the fatigue design of composite structures has been pioneered by Badaliance and Hill [55,56]. However, in recent years Lazzarin and co-workers [57,58] have established that brittle fracture appears to be governed by $\Delta\sqrt{W}$, rather than by ΔW. This finding mirrors the above discussion that delamination growth is governed by $\Delta\sqrt{G}$, rather than by ΔG.

3. EXPERIMENTAL

The CFRP composite material employed, the test specimens and the experimental results from the test programs that are analysed in the present paper have all been previously reported [26,35-37,46], and therefore only the main details are given in the present paper.

The CFRP specimens employed were produced by a hand lay-up process using prepregs made from unidirectional, continuous carbon-fibres in a thermosetting epoxy matrix ('M30SC/DT120' supplied by Delta-Tech S.p.A., Italy).

For the Mode I fatigue tests the DCB specimen was used [49]. The CFRP laminate sheets were either prepared as unidirectional or as multidirectional composites. The unidirectional DCB Mode I specimens were manufactured with lay-up sequences of $[(0)_{12}//(0)_{12}]$, $[(0)_{16}//(0)_{16}]$ and $[(0)_{24}//(0)_{24}]$ composites. These laminates corresponded to specimens with nominal thicknesses of 3.75 mm, 5.0 mm and 7.5 mm, respectively. The multidirectional DCB Mode I specimens were manufactured with a lay-up sequence of $[(\pm45/0_{12}/\mp45)//(\pm45/0_{12}/\mp45)]$ to give a nominal specimen thickness of 5.0 mm. In all cases a 12.7 μm thick film of poly(tetrafluoroethylene) ('Teflon', Du Pont, USA) was inserted into the mid-plane of the laminate DCB specimens during the hand lay-up process to act as an initial delamination, or 'starter crack', of length, a_0, of 44.5 mm. Prior to measurements from the cyclic-fatigue fracture test being taken, this initial delamination in the

specimens was grown to a pre-crack length of a_p to form a natural crack front under quasi-static loading of the specimen.

For any given Mode I DCB test, the test program that was employed involved growing the crack under fatigue loading for a relatively short, distance from the initial value of the pre-crack extension length, a_p-a_0, whilst taking readings of the number of cycles, crack length, load and displacement. The fatigue test was then halted and repeated, but now with respect to the new, longer, crack that was present in the DCB specimen, i.e. the crack length a-a_0 that was now present was taken to be equivalent to the pre-crack extension length, a_p-a_0, for the repeated fatigue test. Thus, a key variable reported in the literature [35-37,46] from the test program using a given DCB specimen was the value of the pre-crack extension length, i.e. the crack extension, a_p-a_0, prior to measurements from a cyclic-fatigue fracture test being taken. It should be noted that, if a pre-crack extension length of a_p-a_0 is not used in the fracture-mechanics test then optimistically high values of the toughness and fatigue resistance will be measured. This is because the starter crack film, of length a_0, represents a relatively blunt crack tip compared to that of a pre-crack which is naturally-grown ahead from the starter film prior to the commencement of the test. However, as will be shown below, fibre-bridging, and hence retardation of the FCG, is seen to arise even for the smallest values of the pre-crack extension length, a_p-a_0, that are typically employed. Hence, the measurement of a statistically valid and 'retardation-free' FCG rate curve directly from fracture-mechanics tests undertaken in the laboratory is fraught with difficulties.

For the Mode II fatigue tests the central cut-ply specimen was employed [26]. These Mode II specimens were manufactured with a lay-up sequence of ten unidirectional plies to give a nominal specimen thickness of 1.56 mm.

For these fatigue tests, various values of the R-ratio were used; where the R-ratio was defined as $R = F_{min}/F_{max}$, where F_{min} and F_{max} were the minimum and maximum loads, respectively, that were applied during the fatigue test. Displacement-control of the test specimens was used for these fatigue tests. Now, in such a displacement-controlled fatigue test, the applied load will decrease as the fatigue crack propagates. However, in this previously-reported work, the value of the R-ratio, as defined above, did not change significantly during a fatigue test for a given value of a_p-a_0, since only a relatively small amount of crack growth was allowed to occur before the fatigue test was halted. (As noted above, the fatigue test parameters were then re-set and the test repeated with cyclic-fatigue fracture measurements now taken which corresponded to the new, longer value of a_p-

a_0 in the DCB specimen; with such fatigue testing being repeated many times for a given DCB test.) Nevertheless, the fatigue tests were carefully monitored and, if there was any significant difference between the *R*-ratio that was required and the *R*-ratio actually being experienced by the test specimen, the minimum displacement being applied was adjusted by a very small amount to keep the *R*-ratio constant. The values of the *R*-ratio used for the many fatigue tests were varied and are stated below as appropriate. The frequency used for the DCB Mode I fatigue tests was 5 Hz. For the central cut-ply Mode II tests the frequency was varied between 1 and 5 Hz, so as to enable more accurate measurements of the crack length to be made, as needed. It was reported [26] that the Mode II fatigue delamination behaviour for this CFRP was not influenced by such variations in the test frequency.

4. THE *da/dN* VERSUS $\Delta\sqrt{G}$ PLOTS

4.1 Introduction

The existing literature [26,35-37,46] on the fatigue testing of the above 'M30SC/DT120' CFRP are the source of the experimental data for the present paper. For the cyclic-fatigue studies, the data reported was in the form of plots of *da/dN* versus $(\sqrt{G_{max}} - \sqrt{G_{min}})^2$. From Equation (2) this term is equivalent to $(\Delta\sqrt{G})^2$. Therefore, for simplicity, and to be consistent with previous work [2], we have chosen to present the data from the literature in the form of plots of *da/dN* versus $\Delta\sqrt{G}$.

4.2 Effect of the value of pre-crack extension length, a_p-a_o, on the 32 ply unidirectional DCB test data

Figure 1 shows values of logarithmic *da/dN* versus logarithmic $\Delta\sqrt{G_I}$ re-plotted from [36]. The data shown are from one test program (termed here 'Test 1') for a unidirectional DCB Mode I specimen with 32 plies, i.e. a lay-up of $[(0)_{16}//(0)_{16}]$, which gave a nominal thickness of 5.0 mm. They were tested at an *R*-ratio of 0.5. Values are given in the legend for the pre-crack extension length, a_p-a_0, prior to the start of measurements from a fatigue test. As may be seen, the fatigue curves for a given value of a_p-a_0 progressively shift towards the right-hand side of the graph as the length of the pre-crack, a_p-a_0, is increased. This implies that there is a retardation of the FCG rate as the value of a_p-a_0, is increased, i.e. as the value of a_p-a_0 increases, and for a given value of $\Delta\sqrt{G_I}$, the corresponding value of *da/dN* is lower, i.e. the fatigue crack grows slower as the value of a_p-a_0 is increased. These

observations were considered [36,37] to arise from the extent of fibre-bridging behind the crack tip progressively becoming more intense as the value of a_p-a_0 was increased. Such an effect, of fibre-bridging, is well established [16,19,21,59] for quasi-static DCB tests. Evidence for it being the operative mechanism in these fatigue tests was provided by the observation [21] that, if the bridging fibres behind the crack tip were cut, and the fatigue test was repeated, the resulting fatigue curve shifted back towards the left-hand side of the graph. These observations mirror those of Huang and Hull [60] who removed the bridging fibres that had developed behind a quasi-statically tested DCB test specimen of a unidirectional glass-fibre epoxy composite. However, in this case the bridging fibres were removed using a stress-corrosion treatment in a solution of hydrochloric acid. This treatment reduced the relatively high value of the quasi-static fracture energy, G_{Ic}, to that of the value of G_{c0} for the initiation fracture energy for the onset of crack growth.

Figure 2 shows values of logarithmic *da/dN* versus logarithmic $\Delta\sqrt{G_I}$ re-plotted from [36,37]. However, the data shown are now from three test programs (termed here 'Test 1', 'Test 2' and 'Test 3'), for three unidirectional DCB Mode I specimens with 32 plies, i.e. giving a nominal thickness of 5.0 mm, and tested at a *R*-ratio of 0.5. Clearly, the same general trend, as described above, can be observed for all three DCB test specimens. Namely, the fatigue curves for a given value of a_p-a_0 progressively shift towards the right-hand side of the graph as the value of a_p-a_0 is increased, and so the FCG curve is increasingly retarded as the value of a_p-a_0 is increased. Nevertheless, the data in Figure 2 also reveals that, for the three DCB specimens, there is inherent scatter present in such tests, as has been previously widely reported [2,16,19,33]. For example, note that the results from 'Test 3' for an a_p-a_0 value of 24.6 mm do not lie to the right of the data (a) from 'Test 1' for an a_p-a_0 value of 19.5 mm, or (b) from 'Test 2' for an a_p-a_0 value of 20.5 mm. Also, the 'Test 3' data for an a_p-a_0 value of 85.2 mm do not lie to right of the data (a) from 'Test 1' for an a_p-a_0 value of 68.1 mm, or (b) from 'Test 2' for an a_p-a_0 value of 79.5 mm, or (c) from 'Test 2' for an a_p-a_0 value of 64.3 mm. Whether this inherent scatter only arises from the scatter inherent in the extent of fibre-bridging that develops behind the crack tip in the test specimens, or arises from other causes, as discussed above, has not yet been established. However, clearly, any methodology proposed to calculate the fatigue properties, which are then going to serve as the material-allowable properties for design and lifing composite structures, must account for both the fibre-bridging effects and the inherent experimental scatter.

4.3 Effect of thickness of the CFRP specimens on the unidirectional DCB test data

To study the effects of the thickness on the fatigue behaviour of the composite, unidirectional DCB Mode I specimens were manufactured with lay-up sequences of $[(0)_{12}//(0)_{12}]$, $[(0)_{16}//(0)_{16}]$ and $[(0)_{24}//(0)_{24}]$ to give DCB specimens with nominal thicknesses of 3.75 mm, 5.0 mm and 7.5 mm, respectively. These DCB specimens were tested at an *R*-ratio of 0.5 [37]. Again, the test program that was employed enabled the pre-crack extension length, a_p-a_0, prior to the start of measurements from a fatigue test being taken, to be varied. The results are shown in Figure 3 for one DCB specimen for each thickness. Clearly, the same general trend may be observed for all three thicknesses of the DCB test specimens, as described above. Namely, the FCG curves for a given value of a_p-a_0 progressively shift towards the right-hand side of the graph as the value of a_p-a_0 is increased. Thus, there is retardation of the FCG curve as the value of a_p-a_0 is increased. Further, the data in Figure 3 also reveal that (a) there is no significant effect of the thickness of the DCB test specimens on the position of the FCG rate curves, i.e. the relationship between *da/dN* versus $\Delta\sqrt{G_I}$, for a given value a_p-a_0, is not significantly affected by the thickness of the specimen, and (b) there is some inherent scatter that is present in such tests, again as has been previously widely reported [2,16,19,33].

4.4 Effect of *R*-ratio on the 32 ply unidirectional DCB test data

The effect on the *R*-ratio was studied [36] using unidirectional DCB Mode I specimens with 32 plies, i.e. a lay-up of $[(0)_{16}//(0)_{16}]$, which gave a nominal thickness of 5.0 mm. These specimens were tested at *R*-ratios of 0.1 or 0.5. Again, the length of the pre-crack, a_p-a_0, prior to measurements from a fatigue test being taken was varied.

The results are shown in Figure 4 for values of logarithmic *da/dN* versus logarithmic $\Delta\sqrt{G_I}$ re-plotted from [36]. The results are shown for test programs, termed here 'Test 1 *R*=0.1' and 'Test 2 *R*=0.1', for two unidirectional DCB Mode I specimens with 32 plies (i.e. giving a nominal thickness of 5.0 mm) and tested at an *R*-ratio of 0.1. Again the FCG curves for a given value of a_p-a_0 progressively shift towards the right-hand side of the graph as the value of a_p-a_0 is increased, and so there is an increased retardation of the FCG rate as the value of a_p-a_0 is increased. For these results there is a steady and progressive increase in the retardation of the FCG curves as the pre-crack extension length, a_p-a_0, was increased prior to measurements being taken from a fatigue test.

The results for two different *R*-ratios of 0.1 or 0.5 are summarised in Figure 5 [36,37]. Yet again the FCG curves for a given value of a_p-a_0 progressively shift towards the right-hand side of the graph as the value of a_p-a_0 is increased, and thus there is a retardation of the FCG rate as the value of a_p-a_0 is increased. Here again a steady increase in the retardation of the FCG curves is generally observed as the value of a_p-a_0 is increased. It should be noted that there is a clear effect of the value of the *R*-ratio that is employed. The fatigue resistance of the composite is inferior if the higher *R*-ratio of 0.5 is used. This observation is in agreement with previous work [30,31] when the crack driving force (CDF) is taken to be $\Delta\sqrt{G_I}$. Namely, the crack in the DCB specimen subjected to a higher *R*-ratio grows at a faster *da/dN* value. Or put another way, for the specimen subjected to the higher *R*-ratio then a higher value of *da/dN* is recorded for a given value of $\Delta\sqrt{G_I}$.

4.5 Effect of lay-up of the CFRP

The effects on the fatigue delamination growth from the choice of the lay-up of the composite was studied by using multidirectional DCB specimens which were manufactured with a lay-up sequence of $[(\pm 45/0_{12}/\mp 45)//(\pm 45/0_{12}/\mp 45)]$ to give a nominal thickness of the specimens of 5.0 mm. The value of a_p-a_0 prior to measurements from a fatigue test being taken was again varied. The *R*-ratio employed was 0.5.

The results from the multidirectional [35] and the unidirectional [36] DCB specimens are shown in Figure 6. As may be seen, again the FCG rate curves for a given value of a_p-a_0 progressively shift towards the right-hand side of the graph as the value of a_p-a_0, is increased. This means that there is an increased retardation of the FCG as the value of a_p-a_0 is increased, due to fibre-bridging progressively developing as the value of a_p-a_0 is increased. Comparing the two types of lay-up, at the lowest values of a_p-a_0 there appears to be no significant differences in the plots of logarithmic *da/dN* versus logarithmic $\Delta\sqrt{G_I}$. However, at the highest values of a_p-a_0 that were used the multidirectional composite does appear to offer improved fatigue properties as compared to the unidirectional composite. This statement is in accord with the commonly reported observation [21,61] that the degree of fibre-bridging develops more rapidly and is more extensive in multidirectional composites. However, observations on the failure path for these multidirectional DCB test specimens, shown in Figure 6, under fatigue loading revealed that that the bridging fibres were only pulled from the ply on either side of the advancing fatigue crack-tip, and that no

multiple-ply cracking, nor any ply-bridging, was observed to develop during the course of these tests.

4.6 Effect of Mode of Loading

The effect of the mode of loading on the figure behaviour is shown in Figure 7 which presents plots of the logarithmic *da/dN* versus logarithmic $\Delta\sqrt{G_{II}}$ for Mode II loading, re-plotted from [26]. The Mode I results shown, for comparison, are from the test program 'Test 3'. They are for a Mode I DCB specimen, using an *R*-ratio of 0.5, and the values are given in the legend for the pre-crack extension length, a_p-a_0, prior to measurements from the fatigue test being taken, see Figure 2. All the composite laminate specimens possessed a unidirectional lay-up. As may be seen in Figure 7, there is a definite effect of the *R*-ratio used for the Mode II tests upon the fatigue behaviour, especially at relatively low values of $\Delta\sqrt{G_{II}}$, with a greater retardation of the FCG curve being seen as the *R*-ratio is increased. Further, under the Mode II loading the composite is observed to possess far greater fatigue resistance than under Mode I loading. However, since the value of a_p-a_0 was not varied in these Mode II tests, no further comments on the retardation of the FCG curves under such Mode II loadings are possible.

5. THE HARTMAN-SCHIJVE 'MASTER' RELATIONSHIP

From the above discussions there are clearly major practical difficulties in conducting DCB fatigue tests which will yield reliable and valid 'upper-bound', and hence conservative, FCG rate curves, i.e. which are 'retardation-free' and also allow for the inherent scatter seen in such fracture-mechanics tests. Such a valid 'upper-bound' FCG curve, which may act as a material-allowable property, is essential for sound composite development and selection, and for accurate design and sustainment studies.

Therefore, following the successful use of the variant of the Hartman-Schijve equation to analyse the FCG in composites and in adhesively-bonded joints [2,27,30,31,62], the first step is to re-plot Figures 1 to 7 via Equation (3) in terms of *da*/*dN* versus $\left[\frac{\Delta\sqrt{G}-\Delta\sqrt{G_{thr}}}{\sqrt{\{1-\sqrt{G_{max}}/\sqrt{A}\}}}\right]$ in order to see if a single, linear 'master' relationship can be obtained from the results of these fracture-mechanic tests undertaken in the laboratory. The details of the procedure used are given in Appendix A and, as may be seen from Figure 8, a linear 'master' Hartman-Schijve representation is indeed obtained.

The values of A and $\Delta\sqrt{G_{thr}}$ needed to give this single 'master' relationship from each set of experimental test data are summarised in Tables 1 to 4. This single linear 'master' representation captures all the results from Figures 1 to 7. It therefore includes: (a) the effect of the pre-crack extension length, a_p-a_0, used (which was varied in the test programs, as described above), (b) the scatter observed in the test programs employing (nominally) replicate composite specimens, (c) the results from the different *R*-ratios used, (d) the results from the different lay-ups and thicknesses of the composite specimens employed, and (e) the results from the different modes of loading, i.e. Modes I and II. This unique 'master' relationship has a linear correlation coefficient, R^2, of 0.994 and a slope, *n*, which has a relatively low value of about two.

6. DETERMINING THE 'UPPER-BOUND' DESIGN RELATIONSHIP

6.1 Introduction

From our previous work [2], a key question that now arises is whether, by using the Hartman-Schijve equation to obtain the single, linear 'master' relationship shown in Figure 8, a methodology can now be developed which allows us:

(i) To estimate a lower-bound value of the fatigue threshold, $\Delta\sqrt{G_{thr0}}$, when the pre-crack extension length, a_p-a_0, in the cyclic fatigue test tends to zero, i.e. so that no retardation of the FCG rate takes place.

(ii) To quantitatively account for the inherent scatter seen in the fracture-mechanics tests.

(iii) To then calculate a corresponding valid, 'upper-bound' curve for the FCG of the delamination, which excludes any retardation effects on the FCG rate and also takes into account the inherent experimental scatter observed in the fatigue tests. Such a FCG curve would act as an 'upper-bound curve' for (a) material development, characterisation and comparison studies, and (b) design and lifing studies.

To undertake this calculation for the 'upper-bound' FCG rate curve of *da/dN* versus $\Delta\sqrt{G}$ we may use Equation (3). Now, the 'master' relationship shown in Figure 8 has a linear correlation coefficient, R^2, of 0.994; and has a slope, *n*, and an intercept, *D*. The values of these parameters are given later in Table 7 and may be used in Equation (3) for such calculations. However, to employ Equation (3) for our calculations, we also need to know the lower-bound value of the threshold,

$\Delta\sqrt{G_{thr0}}$ and the lower-bound value of the term A, i.e. A_0; where the term A_0 may be taken to be the quasi-static value of the initiation fracture energy, G_{c0}, for the onset of crack growth.

6.2 The value of the fatigue threshold, $\Delta\sqrt{G_{thr0}}$

We need to calculate an approximate lower-bound value for the fatigue threshold, $\Delta\sqrt{G_{thr0}}$, when the pre-crack extension length, a_p-a_0, in the cyclic fatigue test tends to zero, i.e. so that no retardation of the FCG takes place in the test specimen. There are two different methods that can be used, and hence they provide a valuable cross-check on the values obtained. The first method uses the data in Tables 1 to 4 to plot the values of $\Delta\sqrt{G_{thr}}$ versus the corresponding value of a_p-a_0 prior to the start of any measurements being taken from a fatigue test, for a given test program. The value of $\Delta\sqrt{G_{thr0}}$ can then be approximated from the functional relationship between $\Delta\sqrt{G_{thr}}$ and a_p-a_0 by setting the value of a_p-a_0 to zero. Three examples of such plots are shown in Figure 9 (a)-(c) and the value of $\Delta\sqrt{G_{thr0}}$ may be readily deduced from such plots. However, it should be noted that whilst the fit to the data points is quite good, i.e. with R^2 values of greater than 0.97, the fits are not exact. It could be argued that, where the data points deviate from the fitted curve, the values of $\Delta\sqrt{G_{thr}}$ associated with the test should be re-evaluated using a detailed statistical analysis. However, this was not done in the present study. The reason for this was that the authors wished to demonstrate how a simple methodology could be used to assess a large number of tests without needing to resort to the use of complex data-analysis tools. The mean and the standard deviation values so deduced are summarised in Table 5. The second method used to estimate $\Delta\sqrt{G_{thr0}}$ is based on the formulae derived in [39] to account for the effect of fibre bridging on G. Here the value of G at the tip of the delamination, in the absence of fibre bridging, G_{tip}, may be estimated from [39]:

$$G_{tip} = G_{app}.\left[\frac{A_0}{A}\right] \tag{5}$$

where G_{app} is the applied value of G. Thus, values of $\Delta\sqrt{G_{thr}}$ and the corresponding value of A from Tables 1 to 4 were employed together with the mean value of A_0 of 250 J/m^2 see below. The resultant mean and the standard deviation values deduced from using this approach are summarised in Table 6. Now, the results obtained by these two very different methods shown in Tables 5 and 6 reveal that the mean values of $\Delta\sqrt{G_{thr0}}$ are in good agreement, and that the values of $\Delta\sqrt{G_{thr0}}$ minus three standard deviations (see below) are in excellent agreement, i.e. with values of 3.4 and 2.9 $\sqrt{(J/m^2)}$ being deduced, respectively.

6.3 The value of the initiation quasi-static fracture energy, G_{c0}, for the onset of crack growth

Next, the value of the lower-bound value of the term A, i.e. A_0, is required. If this term, A_0, is taken [2] to be equivalent to the quasi-static value of the initiation fracture energy, G_{c0}, for the onset of crack growth, then from the work of Yao et al. [35,36,39,46] its value for all the different Mode I DCB test programs shown in Tables 1 to 4 is 250±45 J/m^2. As a matter of interest, it may also be evaluated by the same method as used to obtain the value of $\Delta\sqrt{G_{thr0}}$, i.e. directly from the Mode I values of A given in Tables 1 to 4 for each test program undertaken on a given DCB specimen; and from such an approach the value of A_0 is 260±50 J/m^2. There is clearly no significant difference in the value of A_0 determined by either route.

6.4 A predicted design/lifing relationship

Let us now consider how to determine a valid, 'upper-bound' FCG rate curve, which is 'retardation-free' (i.e. where no effects from any fibre-bridging occurs) and that bounds the experimental data, and so also allows for the inherent scatter that is invariably recorded in the fracture-mechanics tests. To achieve this it is proposed that the best methodology is to use the Hartman-Schijve variant of the Nasgro equation, i.e. Equation (3), and to adopt the statistical approach suggested in [63-65], i.e. by plotting FCG curves obtained from using values of $\sqrt{G_{thr0}}$ and A_0 corresponding to their mean values minus three standard deviations. It should be noted that by using minus three standard deviations for these terms we have adopted an 'A basis' approach [63-65]. Namely, the mechanical property value that is determined is the value above which at least 99% of the population of values is expected to fall with a confidence of 95%. This value is typically used to design and life a single member where the loading is such that its failure would result in a loss of structural integrity.

The relevant values that have been determined, from Figure 8 and as described above, for the various terms needed for Equation (3) are listed in Table 7. The resulting 'upper-bound' FCG curve predicted is plotted in Figure 10. Also plotted in Figure 10 are all the experimental results from the Mode I fracture-mechanics tests that have been shown in Figures 1 to 6. Now, as may be seen from Figure 10, the 'upper-bound' FCG curve predicted from this proposed methodology does indeed encompass. and bounds, all the experimental data. Figure 10 also reveals that the exponent of the power-law relationship that is associated with the approximately linear region between

logarithmic *da/dN* versus logarithmic $\Delta\sqrt{G_I}$ of the 'upper-bound' FCG curve is significantly reduced. Thus, this 'upper-bound' FCG curve represents the 'worst-case' for the FCG rate data; and no, or very little, retardation of the growth of the delamination is present in this predicted curve.

7. CONCLUSIONS

The introduction by the FAA of a 'slow growth' approach to the certification of polymer-matrix fibre composites has focused attention on the experimental data and the analytical tools needed to assess the growth of delaminations in these materials under cyclic-fatigue loads. Therefore, a main aim of the present paper has been to address the topic of the growth of delaminations under cyclic-fatigue loading using a fracture-mechanics approach. Of direct relevance to using such an approach is the fact that previous studies on actual aircraft components and structures [2,40-44] manufactured using composite laminates have revealed no, or only little, retardation in the fatigue crack growth (FCG) rate of delaminations. Therefore, of course, the FCG test data that is ascertained in the laboratory, and then employed as a material-allowable property to design and life the structure, as well as for the development, characterisation and comparison of composite materials, must also exhibit no, or only minimal, retardation.

Now, in laboratory tests the double-cantilever beam (DCB) test specimen, using a typical carbon-fibre reinforced-plastic (CFRP) aerospace composite, is usually employed to obtain fracture-mechanics data under cyclic-fatigue Mode I loading. However, extensive test data reported previously [26,35-37,46] have shown that when employing the DCB it is extremely difficult to perform cyclic-fatigue tests without extensive fibre-bridging developing across the crack faces. This fibre-bridging leads to significant retardation of the FCG rate. The results from the DCB tests have also been shown to exhibit a relatively large degree of inherent scatter [2,16,19,25,33].

In the present paper, we have therefore focussed on establishing a methodology for estimating an 'upper-bound' FCG curve which is representative of a composite laminate exhibiting no, or only very little, retardation under fatigue loading. We have employed a novel methodology, based on using a variant of the Hartman-Schijve equation, to determine such an 'upper-bound' FCG rate curve which may be thought of as a material-allowable property. No, or very little, retardation of the growth of the delamination is present in this predicted 'upper-bound' FCG curve and it bounds the inherent scatter that arises in such fatigue tests. Indeed, it encompasses all the experimental data, using an 'A basis' statistical approach. Therefore, a conservative FCG curve

may be deduced to provide for material development, characterision and comparative studies, and for design and sustainment studies.

Acknowledgements

The experimental work presented in this paper was performed whilst the first author, Liaojun Yao, was at Delft University of Technology in The Netherlands. In this context Dr. Yao acknowledges financial support from the International Postdoctoral Exchange Fellowship Program, Harbin Institute of Technology, P. R. China and the China Postdoctoral Science Foundation with grants No. 2016M601422 and No. 2017T100231. Dr. Yao has subsequently moved to the Department of Astronautics Science and Mechanics, Harbin Institute of Technology, China.

REFERENCES

1. Federal Aviation Authority, (2010) Airworthiness Advisory Circular No: 20-107B. Change 1. Composite Aircraft Structure, 24/8/2010. https://www.faa.gov/documentLibrary/media/Advisory_Circular/AC_20-107B_with_change_1.pdf
2. Jones R., Kinloch A.J., Michopoulos JG., Brunner AJ., Phan, N., (2017) Delamination growth in polymer-matrix fibre composites and the use of fracture mechanics data for material characterisation and life prediction. Composite Structures, 180, pp. 316-333.
3. Jones R., Peng D., Michopoulos JG., Phan N., Berto F., (2017) On the analysis of bonded step lap joints, Theoretical and Applied Fracture Mechanics, https://doi.org/10.1016/j.tafmec.2017.09.001, in press.
4. Ramkumar RL., Whitcomb JD., (1985) Characterization of Mode I and Mixed-Mode delamination growth in T300/5208 graphite epoxy. ASTM STP 876, pp. 315-335.
5. Bathias, C., Laksimi, A., (1985) Delamination threshold and loading effect in fiber glass epoxy composite. ASTM STP, 876, pp. 217-237.
6. Hojo M., Tanaka K., Gustafson C-G., (1987) Effect of stress ratio on near-threshold propagation of delamination fatigue cracks in unidirectional CFRP. Composites Science and Technology, 29, pp. 273-292.
7. Martin RH., Murri, GB., (1990) Characterization of Mode I and Mode II delamination growth and thresholds in AS4/PEEK composites. ASTM STP, 1059, 251-270.
8. Hojo M., Ochiai S., Aoki T., Ito H., (1994) New simple and practical test method for interlaminar fatigue threshold in CFRP laminates. Proceedings 2nd ECCM-Composites, Testing & Standardization, 13th -15th September, pp. 553-561.
9. Dahlen C., Springer GS., (1994) Delamination growth in composites under cyclic loads. Journal of Composite Materials, 28, pp. 732-781.
10. Hojo M., Ando T., Tanaka M., Adachi T., Ochiai S., Endo Y., (2006) Modes I and II interlaminar fracture toughness and fatigue delamination of CF/epoxy laminates with self-same epoxy interleaf. International Journal of Fatigue, 28, pp. 1154–1165.
11. Brunner AJ., Pinter G., Murphy N., (2009) Development of a standardized procedure for the characterization of interlaminar crack growth in advanced composites under fatigue mode I loading conditions. Engineering Fracture Mechanics, 76, pp. 2678–89.
12. Alderliesten RC., (2009) Damage tolerance of bonded aircraft structures. International Journal of Fatigue, 31, pp. 1024-1030.
13. Rans C., Alderliesten R., Benedictus R., (2011) Misinterpreting the results: How similitude can improve our understanding of fatigue delamination growth. Composites Science and Technology, 71, pp. 230–238.
14. Jones R., Pitt S., Brunner AJ., Hui D., (2012) Application of the Hartman-Schijve equation to represent Mode I and Mode II fatigue delamination growth in composites. Composite Structures, 94, pp. 1343-1351.

15. Stelzer S., Brunner AJ., Argüelles A., Murphy N., Pinter G., (2012) Mode I delamination FCG in unidirectional fibre reinforced composites: development of a standardized test procedure. Composite Science Technology, 72, pp.1102–7.

16. Murri GB., (2013) Evaluation of delamination onset and growth characterization methods under mode I fatigue loading. Langley Research Center, Hampton, Virginia. NASA/TM-2013-217966.

17. Pascoe JA., Alderliesten RC., Benedictus R., (2013) Methods for the prediction of fatigue delamination growth in composites and adhesive bonds - A critical review. Engineering Fracture Mechanics, 112-113, pp. 72-96.

18. Jones R., Stelzer S., Brunner AJ., (2014) Mode I, II and mixed Mode I/II delamination growth in composites. Composite Structures, 110, pp. 317-324.

19. Murri GB., (2014) Effect of data reduction and fiber-bridging on Mode I delamination characterization of unidirectional composites. Journal of Composite Materials, 48, pp. 2413-2424.

20. Jones R., Stelzer S., Brunner AJ., (2014) Mode I, II and mixed mode I/II delamination growth in composites. Composite Structures, 110, pp. 317-324.

21. Yao L., Alderliesten R., Zhao M., Benedictus R., (2014) Bridging effect on mode I fatigue delamination behavior in composite laminates. Composites A, 63, pp. 103-109.

22. Yibing X., Runze L., Tishun P., Yongming L., (2014) A novel sub-cycle composite delamination growth model under fatigue cyclic loadings. Composite Structures, 108, pp. 31-40.

23. Ishbir C., Banks-Sills, L., Fourman V., Eliasi R., (2014) Delamination propagation in a multi-directional woven composite DCB specimen subjected to fatigue loading. Composites Part B: Engineering, 66, pp. 180-189.

24. Khan R., Alderliesten R., Yao L., Benedictus R., (2014) Crack closure and fibre bridging during delamination growth in carbon fibre/epoxy laminates under mode I fatigue loading. Composites A, 124, 67, 201–211.

25. Stelzer S., Brunner AJ., Argüelles A., Murphy N., Cano GM., Pinter G., (2014) Mode I delamination FCG in unidirectional fibre reinforced composites: results from ESIS TC4 round robins. Engineering Fracture Mechanics, 116, pp. 92–107.

26. Rans CD., Atkinson J., Li C., (2015) On the onset of the asymptotic stable fracture region in the Mode II fatigue delamination growth behaviour of composites. Journal of Composite Materials, 49, pp. 685-697.

27. Jones R., Hu W. and Kinloch AJ., (2015) A convenient way to represent FCG in structural adhesives. Fatigue and Fracture of Engineering Materials and Structures, 38, pp. 379-391.

28. Khan R., Alderliesten R., Badshah S., Benedictus R., (2015) Effect of stress ratio or mean stress on fatigue delamination growth in composites: Critical review. Composite Structures, 124, pp. 214–227.

29. Zhao L., Gong Y., Zhang J., Wang Y., Lu Z., Peng L., Hu N., (2016) A novel interpretation of fatigue delamination growth behavior in CFRP multidirectional laminates. Composites Science and Technology, 133, pp. 79-88.

30. Jones R., Kinloch AJ., Hu W., (2016) Cyclic-FCG in composite and adhesively-bonded structures: the FAA slow crack growth approach to certification and the problem of similitude. International Journal of Fatigue, 88, pp. 10-18.

31. Hu W., Jones R., Kinloch AJ., (2016) Discussion of the stress ratio effect on the fatigue delamination growth characterization in FRP composite structures. Procedia Structural Integrity, 2, pp. 66-71.

32. Yao L., Alderliesten RC., Benedictus R., (2016) The effect of fibre bridging on the Paris relation for mode I fatigue delamination growth in composites. Composite Structures, 140, pp. 125-135.

33. Brunner AJ., Stelzer S., Pinter G., Terrasi GP., (2016) Cyclic fatigue delamination of carbon fiber-reinforced polymer-matrix composites: data analysis and design considerations. International Journal of Fatigue, 83, pp. 293-299.

34. Mujtaba A., Stelzer S., Brunner AJ., Jones R., (2017) Influence of cyclic stress intensity threshold on the scatter seen in cyclic Mode I fatigue delamination growth in DCB tests. Composite Structures, 169, pp. 138-143.

35. Yao L., Sun Y., Alderliesten RC., Benedictus R., Zhao M., (2017) Fibre bridging effect on the Paris relation for mode I fatigue delamination growth in composites with consideration of interface configuration. Composite Structures, 159, pp. 471-478.

36. Yao L., Sun Y., Zhao M., Alderliesten RC., Benedictus R., (2017) Stress ratio dependence of fibre bridging significance in mode I fatigue delamination growth of composite laminates. Composites A, 95, pp. 65-74.

37. Yao L., Sun Y., Guo L., Alderliesten RC., Benedictus R., Zhao M., Jia, L., (2017) Fibre bridging effect on the Paris relation on mode I fatigue delamination in composite laminates with different thicknesses. International Journal of Fatigue, 103, pp. 196-206.

38. Simon, I., Banks-Sills L., Fourman, V., (2017) Mode I delamination propagation and R-ratio effects in woven DCB specimens for a multi-directional layup. International Journal of Fatigue, 96, pp. 237-251.

39. Yao L., Sun Y., Guo L., Zhao M., Jia, L., Alderliesten RC., Benedictus R., (2017) A modified Paris relation for fatigue delamination with fibre bridging in composite laminates. Composite Structures, 176, pp. 556-564.

40. Molent L., Forrester C., (2017) Lead crack concept applied to defect growth in aircraft composite structures. Composite Structures, 166, pp. 22–26.

41. Berens AP., Hovey PW., Skinn DA., (1991) Risk analysis for aging aircraft fleets - Volume 1: Analysis. WL-TR-91-3066, Flight Dynamics Directorate, Wright Laboratory, Air Force Systems Command, Wright-Patterson Air Force Base, USA. http://www.dtic.mil/dtic/tr/fulltext/u2/a587824.pdf

42. Brussat T., (2013) When ‘What we always do’ won't solve the problem, Lincoln Presentation, ASIP 2013, Bonita Springs, Florida, December 3rd-5th,, available on line at; http://www.meetingdata.utcdayton.com/agenda/asip/2013/agenda.htm.

43. Mandell, JF., Agastra P., Cairns, DS., Badaliance, R., Sears, A., Damage threshold characterization in structural composite materials and composite joints, Final Technical Report, for FA9550-06-1-0444, AFOSR/DEPSCOR 06. www.dtic.mil/cgi-bin/GetTRDoc?AD=ADA516534&Location=U2&doc.pdf

44. Clark G., van Blaricum TJ., (1987) Load spectrum modification effects on fatigue of impact damaged, carbon fibre composite coupons. Composites,18, pp. 243–51.

45. Hartman, A., Schijve J., (1970) The effects of environment and load frequency on the crack propagation law for macro FCG in aluminum alloys. Engineering Fracture Mechanics, 1, pp. 615-631.

46. Sun Y., Yao L., Alderliesten RC., Benedictus R., (2016) Mode I quasi-static delamination growth in multidirectional composite laminates with different thicknesses. Proceedings 31st Technical Conference, American Society for Composites, pp. 1115-1125.

47. Wang, SS., Mandell, JF., McGarry, J. (1978) Analysis of crack tip stress-field in DCB adhesive fracture specimens. International Journal of Fracture 14, pp. 39-58.

48. Tvergaard, V., Hutchinson, JW. (1993) The influence of plasticity on mixed mode interface toughness. Journal Mechanics and Physics of Solids 41, pp. 1119-1135.

49. International Test Standard (ISO), (2001) Fibre-reinforced plastic composites - Determination of mode I interlaminar fracture toughness, GIC, for unidirectionally reinforced materials, ISO 15024:2001, Switzerland.

50. Paris PC., Gomez RE., Anderson WE., (1961) A rational analytic theory of fatigue. The Trend in Engineering, 13/1, pp. 9-14.

51. Paris PC., Erdogan F., (1963) Critical analysis of crack growth propagation laws. ASME Transactions Journal Basic Engineering, 85D, pp. 528-534.

52. Paris PC., (2014) A brief history of the crack tip stress intensity factor and its application. Meccanica, 49, pp. 759–764.

53. Sih, GC., Paris PC., and Irwin GR., (1965) On cracks in rectilinearly anisotropic bodies. International Journal of Fracture Mechanics, 1, pp.189-203.

54. Forman, RG., Mettu, SR. (1992) Behavior of surface and corner cracks subjected to tensile and bending loads in Ti-6Al-4V alloy. ASTM STP, 1131, pp. 519-546.

55. Badaliance, R., Dill, HD. (1979) Compression fatigue life prediction methodology for composite structures, Vol. II, McDonnell Aircraft Co., Report No. MDC-A573, USA.

56. Badaliance, R., Dill, HD. (1982) Damage mechanism and life prediction of graphite-epoxy composites. ASTM STP 775, pp. 229-42.

57. Berto F., Lazzarin P., (2014) Recent developments in brittle and quasi-brittle failure assessment of engineering materials by means of local approaches, Materials Science and Engineering R: Reports, 75 pp. 1–48.

58. De Monte M., Quaresimin M., Lazzarin P., (2007) Modelling of fatigue strength data for a short fiber reinforced polyamide 6.6 based on local strain energy density, in Proceedings of ICCM16, 16th International Conference on Composite Materials, pp. 8–14 July, Kyoto, Japan.

59. Hashemi S., Kinloch AJ., Williams JG., (1990) The effects of geometry, rate and temperature on the Mode I, Mode II and Mixed-mode I/II interlaminar fracture of carbon-fibre/poly(ether-ether ketone) composites. Journal of Composite Materials, 24, pp. 918-956.

60. Huang XN., Hull D., (1989) Effects of fibre bridging on G_{IC} of a unidirectional glass/epoxy composite. Composites Science and Technology, 35, pp. 283-299.

61. Choi NS., Kinloch AJ., Williams JG., (1999) Delamination fracture of multidirectional carbon-fibre/ epoxy composites under Mode I, Mode II and Mixed-Mode I/II loading. Journal of Composite Materials, 33, pp. 73-100.

62. Hu W., Jones, R., Kinloch, AJ., (2016) Computing the growth of naturally-occurring disbonds in adhesively-bonded joints. Engineering Fracture Mechanics, **152**, pp. 162-173.

63. Niu, M.C.Y., (1992) Composite airframe structures: Practical design information and data. Conmilit Press, Hong Kong.

64. Rouchon J., (2009) Fatigue and damage tolerance evaluation of structures: the composite materials response, 22nd Plantema Memorial Lecture, 25th ICAF Symposium, Hamburg, Germany, Rotterdam, The Netherlands, National Aerospace Laboratory NLR, NLR-TP-2009-221. https://reports.nlr.nl/xmlui/bitstream/handle/10921/224/TP-2009-221.pdf?sequence=1

65. Battelle Memorial Institute, (2013) Metallic Materials Properties Development and Standardization (MMPDS) Handbook-08, USA. https://www.sae.org/publications/books/content/b-965/

APPENDIX A: DETERMINING THE VALUES OF A AND $\Delta\sqrt{G_{thr}}$

As explained in [2,18,27,30] and in the main body of the present paper, the values of A and $\Delta\sqrt{G_{thr}}$ are best chosen so as to ensure that Equation (3) fits an experimental set of test data of logarithmic *da/dN* versus logarithmic $\Delta\sqrt{G}$ over the entire range of FCG rates. In this context [2] noted that, when using Equation (3) to obtain a linear 'master' relationship from a given set of test data of *da/dN* versus $\Delta\sqrt{G}$, then the value of A to be employed corresponded to the quasi-static value of the initiation fracture energy, G_{c0}, for the onset of crack growth. In [2] we analysed the test data presented in [19] for ten replicate DCB tests associated with delamination growth in an IM7/977-3 CFRP and in [16,19] for twenty-three replicate DCB tests associated with delamination growth in an IM7/8552 CFRP, and we used the values for G_{c0} given in [16,19]. Thus, the linear 'master' relationship representation for these two different CFRPs, using Equation (3), was obtained by merely choosing the appropriate values of $\Delta\sqrt{G_{thr}}$ for each of the ten tests associated with the IM7/977-3 composite and the twenty-three tests associated with the IM7/8552 composite. Despite the large scatter seen in the FCG curves associated with the twenty-three IM7/8552 curves, by merely allowing for changes in the term $\Delta\sqrt{G_{thr}}$ the Hartman-Schijve equation was able to collapse these twenty-three different tests onto a single, linear 'master relationship. Similarly, despite the large scatter seen in the FCG curves associated with the ten replicate IM7/977-3 specimens, by merely allowing for changes in the term $\Delta\sqrt{G_{thr}}$ the Hartman-Schijve equation was again able to collapse these ten different tests onto a single, linear 'master' relationship. The situation in the fifty-nine tests using the M30SC/DT120 CFRP studied in the present paper is slightly different, in that the values of A for each of these tests are unknown. Therefore, the values of A and $\Delta\sqrt{G_{thr}}$ were chosen so that, for a given set of test data, the logarithmic *da/dN* versus logarithmic $\left[\frac{\Delta\sqrt{G}-\Delta\sqrt{G_{thr}}}{\sqrt{\{1-\sqrt{G_{max}}/\sqrt{A}\}}}\right]$ plots, as given by Equation (3), became virtually linear. After each individual linear relationship for a given set of test data points had been determined, a combined plot of each of these different fifty-nine tests was assembled. This plot is shown in Figure 8. Here it can be seen that, allowing for experimental error, the resultant fifty-nine curves are in good agreement, and enable a single, linear 'master' relationship to be defined Hence, although the agreement might be improved by slightly varying the values of the terms A and $\Delta\sqrt{G_{thr}}$ associated with each of these fifty-nine tests, it was decided to employ these values in Equation (3) without any additional minor

adjustments. These values are shown in Tables 1-4. This one linear ‘master’ relationship that may be readily fitted to all the fifty-nine sets of data shown in Figure 8 has a linear correlation coefficient, R^2, of 0.994. Values of the slope, *n*, and intercept, *D*, of this ‘master’ relationship are given in Table 6, and are subsequently used to predict the ‘upper-bound’ FCG rate curve, as described above.

APPENDIX B: THE MATHEMATICAL RELATIONSHIP BETWEEN $\Delta\sqrt{G_{thr}}$ AND $\Delta\sqrt{G_{th}}$

The Hartman-Schijve variant of the Nasgro equation used in this paper takes the form:

$$\frac{da}{dN} = D\left[\frac{\Delta\sqrt{G}-\Delta\sqrt{G_{thr}}}{\sqrt{\{1-\sqrt{G_{max}}/\sqrt{A}\}}}\right]^n \qquad \text{(B1)}$$

It is important to note that the term $\Delta\sqrt{G_{thr}}$ differs from the quantity $\Delta\sqrt{G_{th}}$, which corresponds to the value of $\Delta\sqrt{G}$ associated with a delamination growth rate, *da/dN*, of 10^{-10} m/cycle. The use of $\Delta\sqrt{G_{th}}$ in equation (B1) is inappropriate. Since, at $\Delta\sqrt{G} = \Delta\sqrt{G_{th}}$ then equation (B1) would return a value of *da/dN* that is zero instead of the required value of *da/dN* = 10^{-10} m/cycle. Therefore, the term $\Delta\sqrt{G_{thr}}$ is introduced to ensure that at $\Delta\sqrt{G} = \Delta\sqrt{G_{th}}$ the value of *da/dN* is equal to 10^{-10} m/cycle. Hence, the values of $\Delta\sqrt{G_{thr}}$ and $\Delta\sqrt{G_{th}}$ are related by Equation (B2), viz:

$$10^{-10} = D\left[\frac{\Delta\sqrt{G_{th}}-\Delta\sqrt{G_{thr}}}{\sqrt{\{1-\sqrt{G_{max}}/\sqrt{A}\}}}\right]^n \qquad \text{(B2)}$$

To illustrate the magnitude of the difference, which is generally very small, let us consider the predicted upper-bound FCG curve shown in Figure 10. In this instance D = 1.73 x 10^{-8}, n = 2.22, *A* = 115 J/m^2, and $\Delta\sqrt{G_{thr}}$ = 3.2 √(J/m^2). This yields a value of $\Delta\sqrt{G_{th}}$ = 3.3 √(J/m^2), a difference of 0.1 √(J/m^2) compared to the value of $\Delta\sqrt{G_{thr}}$. Thus, as can be seen, the difference between the values of $\Delta\sqrt{G_{thr}}$ and $\Delta\sqrt{G_{th}}$ is indeed very small. Nevertheless, from a mathematical and an engineering perspective, it is better to use $\Delta\sqrt{G_{thr}}$, and not $\Delta\sqrt{G_{th}}$, in Equation (3) (i.e. Equation (B1)), otherwise unnecessary errors can be introduced at low delamination FCG rates.

Table 1. Values of $\Delta\sqrt{G_{thr}}$ and A used to obtain the linear 'master' relationship shown in Figure 8 for the results shown in Figures 1 and 2.

Ply configuration, and (a_p-a_0) in mm	R-ratio	$\Delta\sqrt{G_{thr}}$ ($\sqrt{(J/m^2)}$)	A (J/m^2)
Mode I			
$[(0)_{16}//(0)_{16}]$ ('Test 1')			
3.4	0.5	5.5	300
11.6	0.5	6.9	330
19.5	0.5	7.8	390
26.6	0.5	8.3	500
37.2	0.5	8.9	550
47.5	0.5	8.9	610
59.8	0.5	9.5	690
68.1	0.5	9.9	700
$[(0)_{16}//(0)_{16}]$ ('Test 2')			
4.1	0.5	5.8	260
12.7	0.5	6.4	280
20.5	0.5	8.0	400
27.7	0.5	8.4	420
39.5	0.5	9.2	550
51.3	0.5	9.3	610
64.3	0.5	9.8	695
79.5	0.5	9.9	710
$[(0)_{16}//(0)_{16}]$ ('Test 3')			
2.7	0.5	5.8	280
11.6	0.5	6.7	400
24.6	0.5	7.7	425
37.2	0.5	8.2	520
49.6	0.5	9.4	680
58.1	0.5	9.4	700
85.2	0.5	9.7	710

Table 2. Values of $\Delta\sqrt{G_{thr}}$ and A used to obtain the linear 'master' relationship shown in Figure 8 for the results shown in Figure 3.

Ply configuration, and (a_p-a_0) in mm	R-ratio	$\Delta\sqrt{G_{thr}}$ ($\sqrt{(J/m^2)}$)	A (J/m^2)
Mode I			
$[(0)_{24}//(0)_{24}]$ (Thickness = 7.5 mm)			
3.1	0.5	5.5	240
12.5	0.5	6.1	250
20.4	0.5	6.1	310
31.0	0.5	7.4	600
39.8	0.5	8.3	500
54.4	0.5	8.6	580
69.6	0.5	9.6	700
83.9	0.5	9.6	680
101.2	0.5	9.7	700
$[(0)_{16}//(0)_{16}]$ (Thickness = 5.0 mm)			
2.7	0.5	5.8	280
11.6	0.5	6.7	400
24.6	0.5	7.7	425
37.2	0.5	8.2	520
49.6	0.5	9.4	680
58.1	0.5	9.4	700
85.2	0.5	9.7	710
$[(0)_{12}//(0)_{12}]$ (Thickness = 3.75 mm)			
1.3	0.5	6.0	290
10.4	0.5	6.8	380
20.9	0.5	7.9	480
27.7	0.5	7.0	500
35.5	0.5	8.7	550
48.9	0.5	9.5	620
58.3	0.5	9.4	620

Table 3. Values of $\Delta\sqrt{G_{thr}}$ and A used to obtain the linear 'master' relationship shown in Figure 8 for the results shown in Figures 4 and 5.

Ply configuration, and (a_p-a_0) in mm	R-ratio	$\Delta\sqrt{G_{thr}}$ ($\sqrt{(J/m^2)}$)	A (J/m^2)
Mode I			
$[(0)_{16}//(0)_{16}]$ 'Test 1 R=0.1'			
2.7	0.1	9.2	240
14.8	0.1	10.5	350
28.0	0.1	12.9	570
40.0	0.1	14.5	680
53.6	0.1	16.4	700
$[(0)_{16}//(0)_{16}]$ 'Test 2 R=0.1'			
4.1	0.1	9.6	250
16.5	0.1	10.1	625
43.8	0.1	15.1	900
60.3	0.1	16.1	2000
79.6	0.1	16.7	2920

Table 4. Values of $\Delta\sqrt{G_{thr}}$ and A used to obtain the linear 'master' relationship shown in Figure 8 for the results shown in Figures 6 and 7.

Ply configuration, and (a_p-a_0) in mm	R-ratio	$\Delta\sqrt{G_{thr}}$ ($\sqrt{(J/m^2)}$)	A (J/m^2)
Mode I			
$[(\pm45/0_{12}/\mp45)//(\pm45/0_{12}/\mp45)]$			
3.3	0.5	5.2	165
9.0	0.5	7.2	300
20.9	0.5	9.6	650
29.0	0.5	9.8	780
38.0	0.5	10.1	1200
51.3	0.5	11.8	1370
62.8	0.5	11.6	1370
Mode II			
$[(0)_5//(0)_5]$			
	0.5	14.2	1700
	0.3	14.5	1700
	0.1	17.2	1700

Table 5 The mean value and the standard deviation of the term $\Delta\sqrt{G_{thr0}}$ as determined from all the Mode I DCB test programs given in Tables 1 to 4, using the approach illustrated in Figure 9.

Mean ($\sqrt{(J/m^2)}$)	5.2
Standard deviation ($\sqrt{(J/m^2)}$)	0.6
Mean - 3 standard deviations ($\sqrt{(J/m^2)}$)	3.4

Table 6 The mean value and the standard deviation of the term $\Delta\sqrt{G_{thr0}}$ as determined from all the Mode I DCB test programs given in Tables 1 to 4, using the approach given in [39].

Mean ($\sqrt{(J/m^2)}$)	3.8
Standard deviation ($\sqrt{(J/m^2)}$)	0.3
Mean - 3 standard deviations ($\sqrt{(J/m^2)}$)	2.9

Table 7. Values of the terms employed in Equation (3) used to predict the 'upper-bound' FCG curve shown in Figure 10.

Term	Value
D	1.73×10^{-8}
n	2.22
$\Delta\sqrt{G_{thr0}}$ - 3 standard deviations	3.2 $\sqrt{(J/m^2)}$
G_{c0} - 3 standard deviations (where $G_{c0} = A_0$)	115 J/m^2

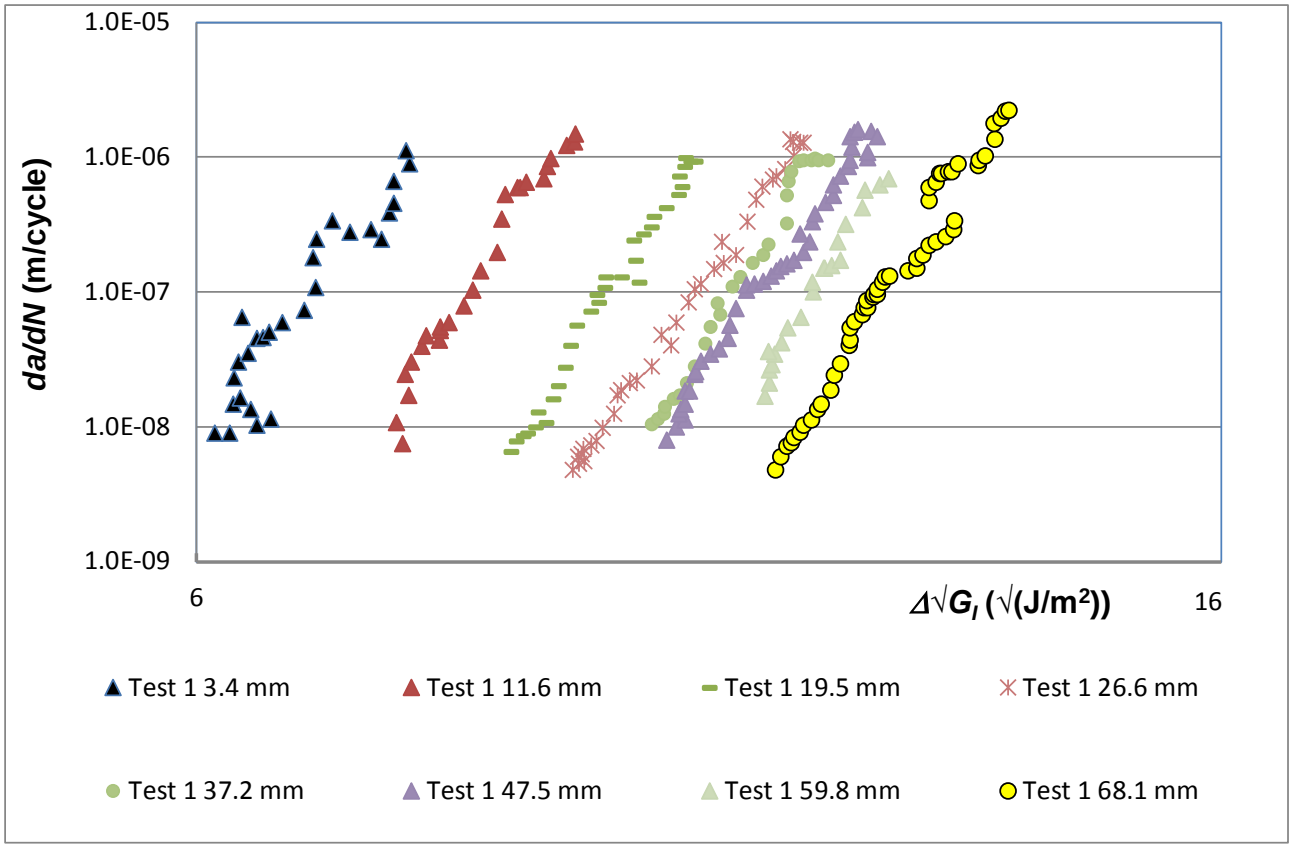

Figure 1. The values of logarithmic *da/dN* versus logarithmic $\Delta\sqrt{G_I}$ re-plotted from [36] are for one unidirectional DCB Mode I specimen consisting of 32 plies (i.e. giving a nominal thickness of 5.0 mm) and tested at an *R*-ratio of 0.5. Values are given in the legend for the pre-crack extension length, a_p-a_0, prior to the start of measurements from a fatigue test. (The data are termed as being from test program: 'Test 1'.)

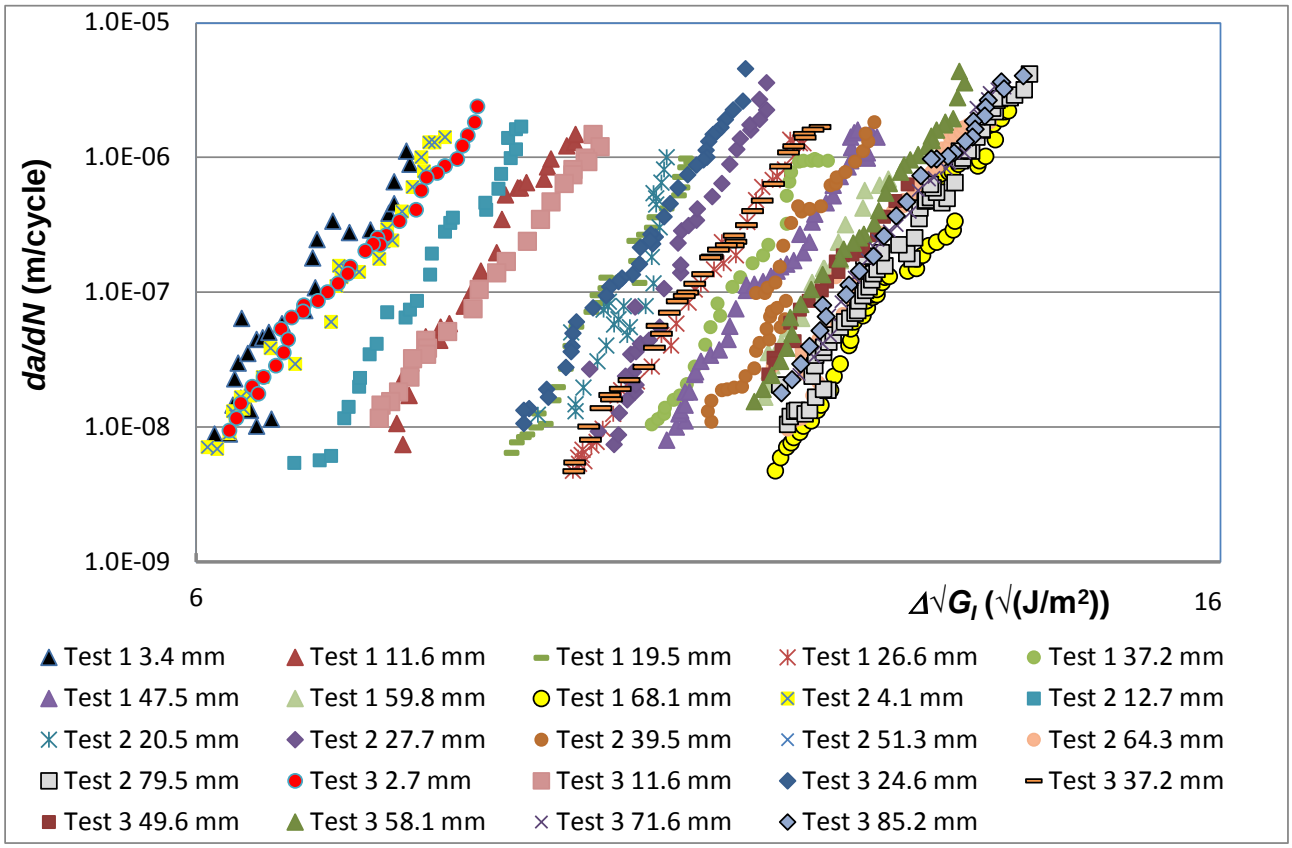

Figure 2. Values of logarithmic *da/dN* versus logarithmic $\Delta\sqrt{G_I}$ re-plotted from [36,37] showing the effects of the scatter from three test programs, termed: 'Test 1', 'Test 2' and 'Test 3'. The three unidirectional DCB Mode I test specimens were made using 32 plies (i.e. giving a nominal thickness of 5.0 mm) and tested at an *R*-ratio of 0.5. Values are given in the legend for the pre-crack extension length, a_p-a_0, prior to the start of measurements from a fatigue test.

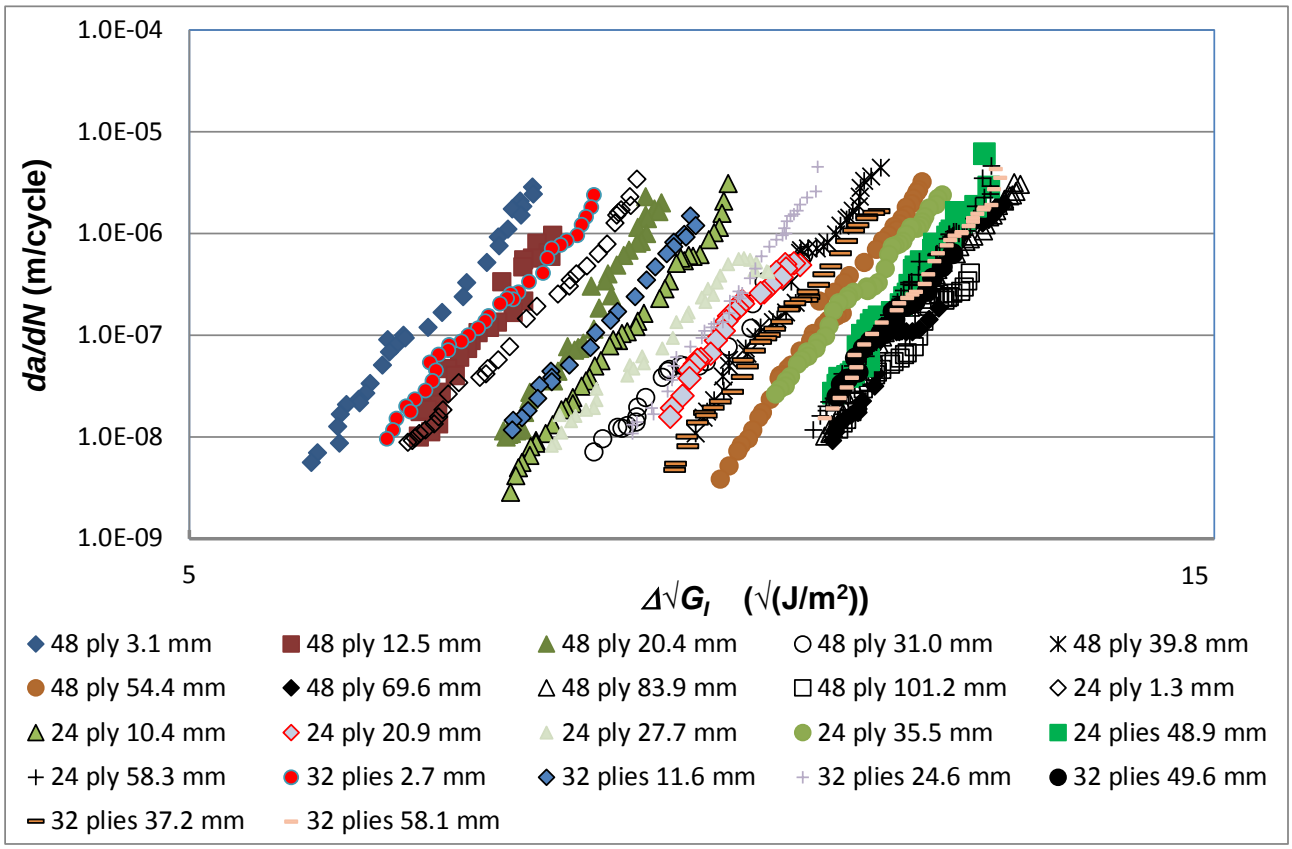

Figure 3. Values of logarithmic *da/dN* versus logarithmic $\Delta\sqrt{G_I}$ re-plotted from [37] showing the effects of the thickness of the unidirectional DCB Mode I specimens, tested at an *R*-ratio of 0.5. Values are given in the legend for the pre-crack extension length, a_p-a_0, prior to the start of measurements from a fatigue test. (For the unidirectional DCB Mode I specimen that was made using 32 plies the data are from the test program: 'Test 3', see Figure 2.)

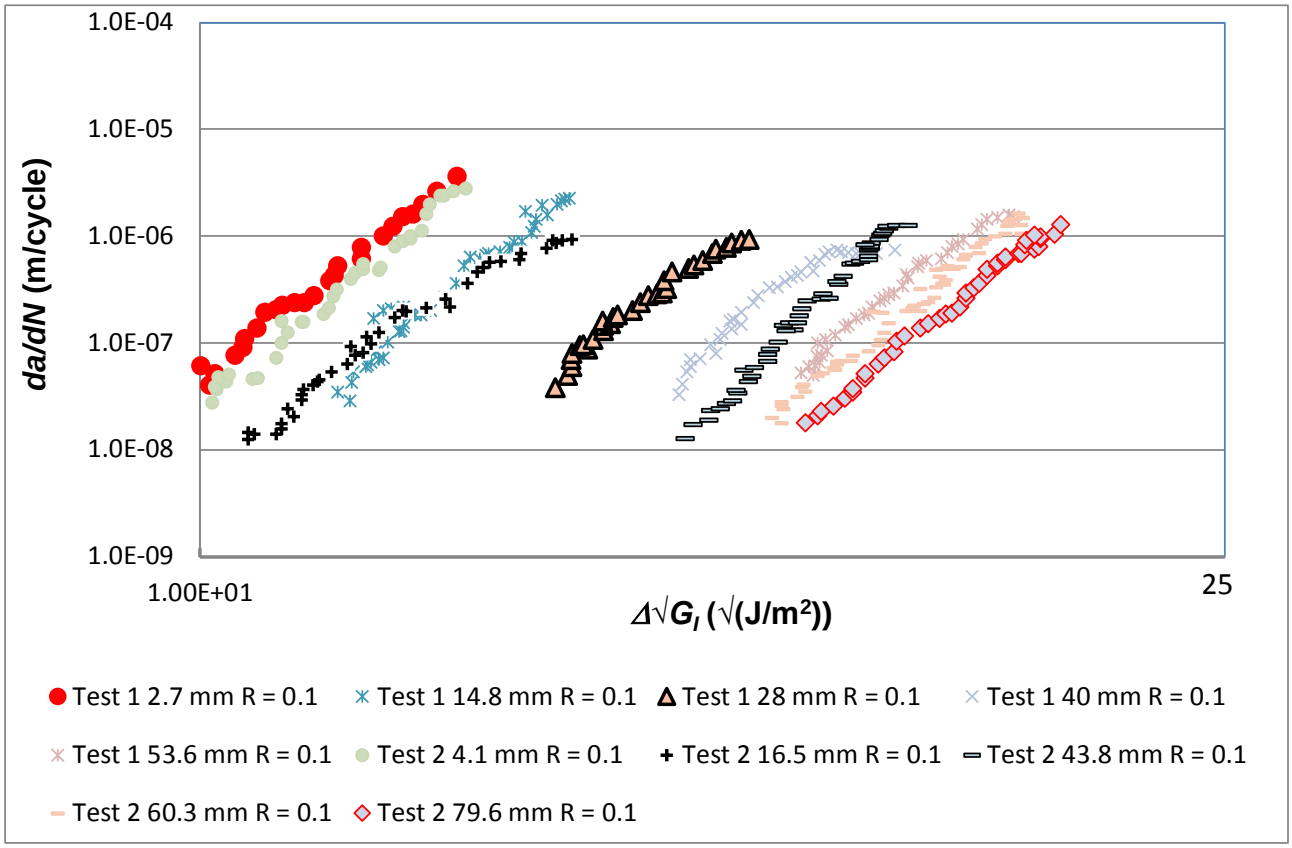

Figure 4. Values of logarithmic *da/dN* versus logarithmic $\Delta\sqrt{G_I}$ re-plotted from [36] showing results from two unidirectional DCB Mode I specimens tested at an *R*-ratio of 0.1. The results are termed as being from test programs: 'Test 1 *R*=0.1' and 'Test 2 *R*=0.1'. The two unidirectional DCB Mode I specimens were made using 32 plies (i.e. giving a nominal thickness of 5.0 mm). Values are given in the legend for the pre-crack extension length, a_p-a_0, prior to the start of measurements from a fatigue test.

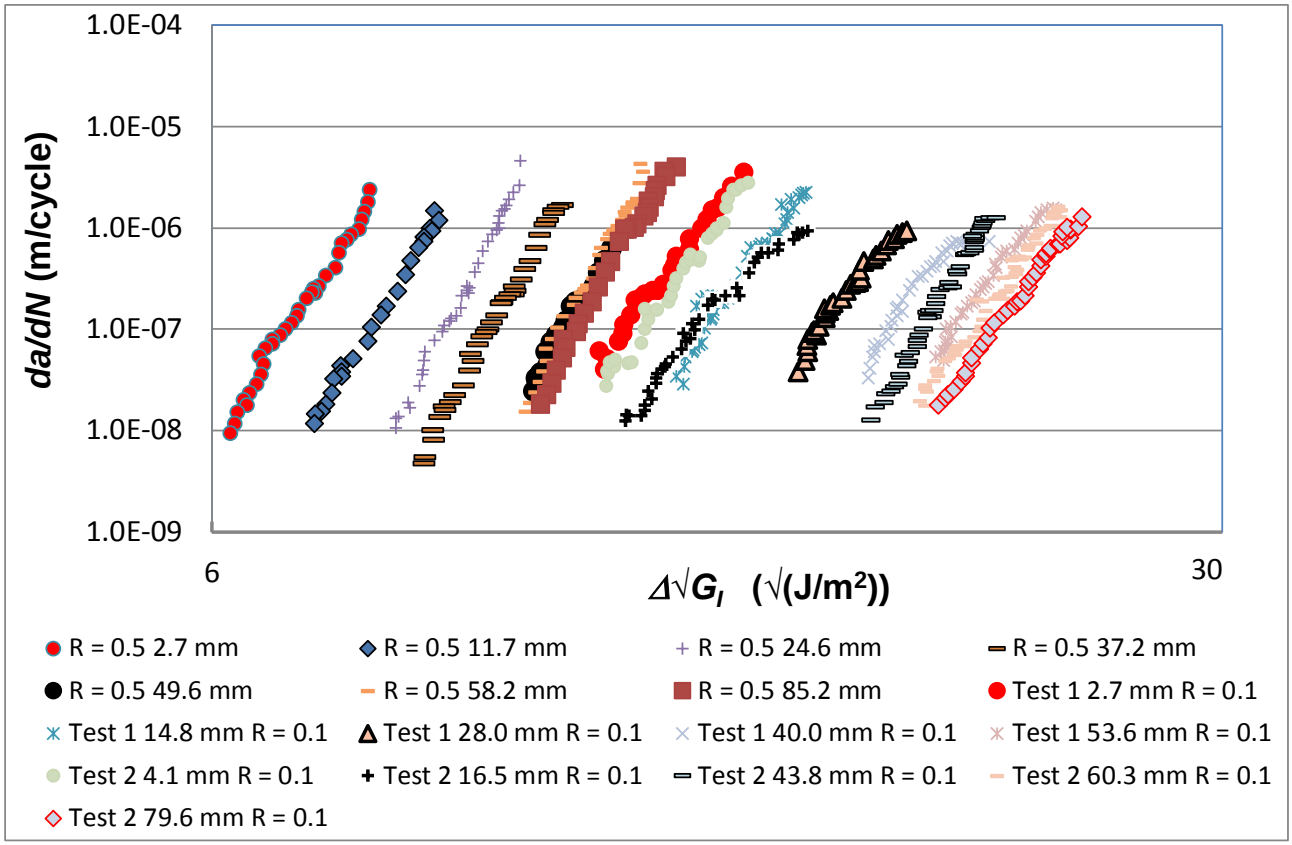

Figure 5. Values of logarithmic *da/dN* versus logarithmic $\Delta\sqrt{G_I}$ re-plotted from [36,37] showing the effect of the *R*-ratio employed. Data are given for two test programs: 'Test 1 *R*=0.1' and 'Test 2 *R*=0.1', which are from two unidirectional DCB Mode I specimens made using 32 plies (i.e. giving a nominal thickness of 5.0 mm) and tested at an *R*-ratio of 0.1, see Figure 4. Also shown are the data for a similar DCB specimen but tested at an *R*-ratio of 0.5, see Figure 2 and the 'Test 3' program. Values are given in the legend for the pre-crack extension length, a_p-a_0, prior to the start of measurements from a fatigue test.

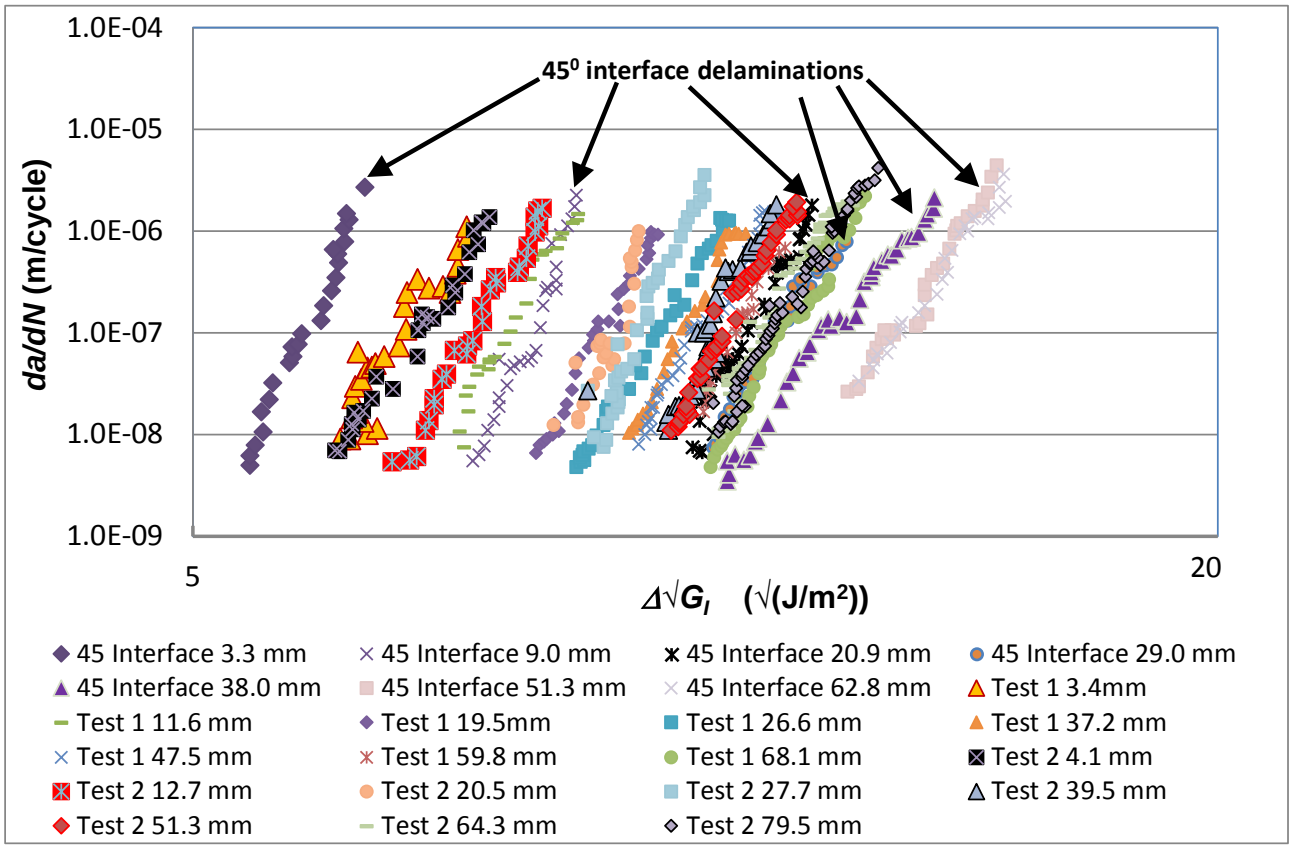

Figure 6. Values of logarithmic *da/dN* versus logarithmic $\Delta\sqrt{G_I}$ re-plotted from [35] showing the effect of the lay-up of the composite. Data are from a test program using a multidirectional DCB Mode I specimen made using 32 plies (i.e. giving a nominal thickness of 5.0 mm) with the fatigue crack growing along the $45^o/45^o$ interface. Data are also given [36] for two unidirectional DCB Mode I specimens made using 32 plies (i.e. giving a nominal thickness of 5.0 mm) and are the results from the test programs: 'Test 1' and 'Test 2', see Figure 2. Values are given in the legend for the pre-crack extension length, a_p-a_0, prior to the start of measurements from a fatigue test. All the tests were conducted at an *R*-ratio of 0.5.

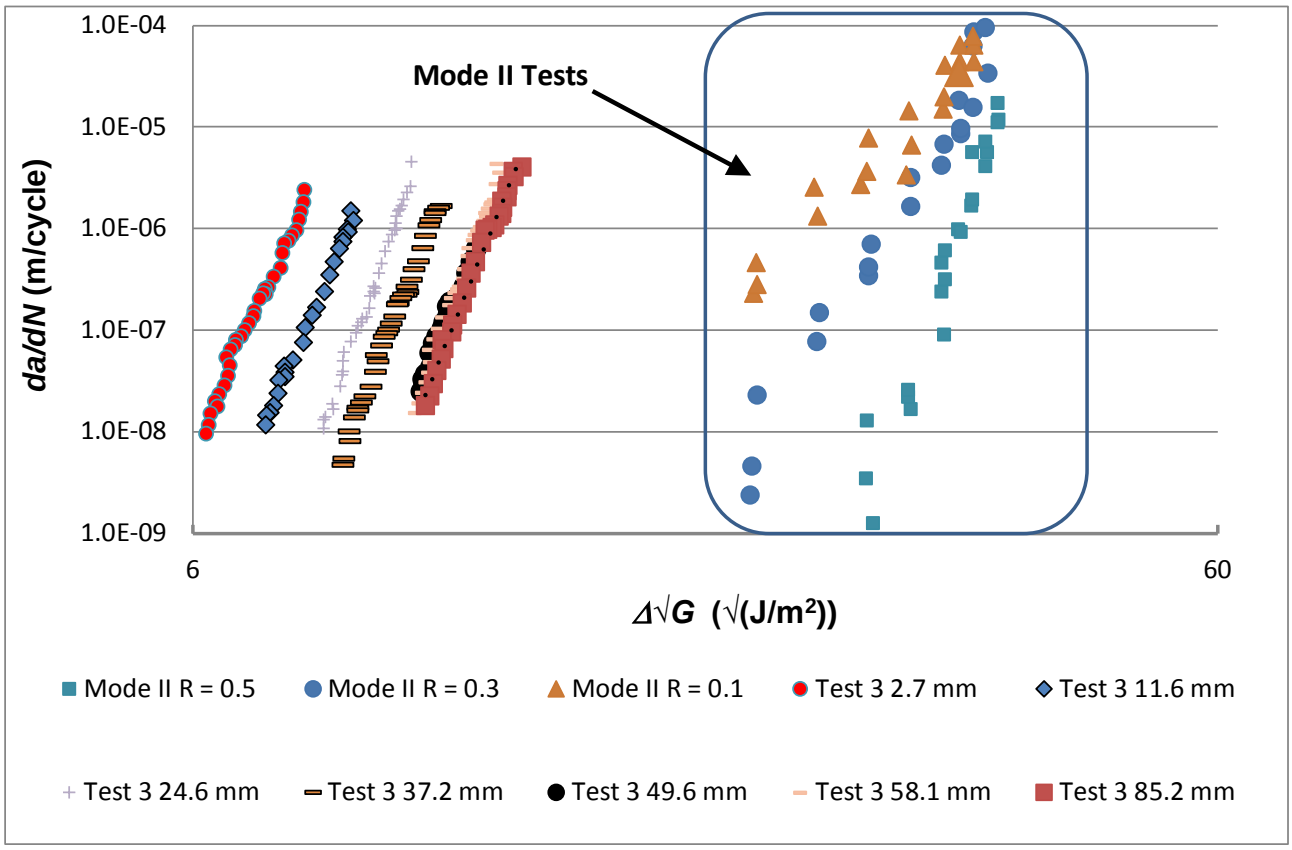

Figure 7. Values of logarithmic *da/dN* versus logarithmic $\Delta\sqrt{G}$ re-plotted from [26,37] showing results for Mode II and Mode I loadings. The Mode I results, shown for comparison, are for a DCB specimen using an *R*-ratio of 0.5, see Figure 2 and the test program: 'Test 3'. The values given in the legend are for the pre-crack extension length, a_p-a_0, prior to the start of measurements from the DCB specimen. All the composite specimens possessed a unidirectional lay-up.

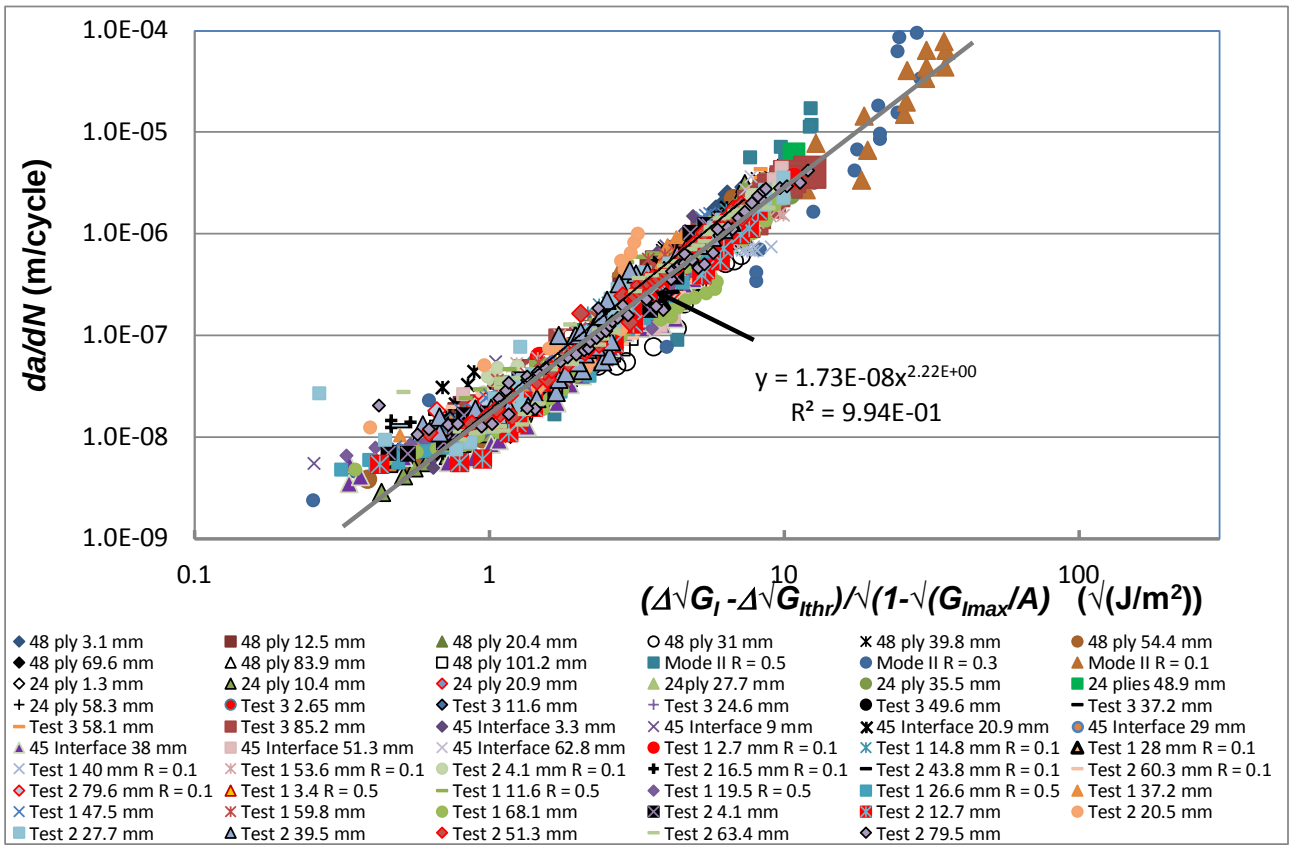

Figure 8. The single, linear 'master' relationship obtained for all the many sets of test data shown in Figures 1 to 7. This 'master' relationship was calculated using the Hartman-Schijve equation, Equation (3). The values of A and $\Delta\sqrt{G_{thr}}$ needed for each set of laboratory test data to give the 'master' relationship, using Equation (3), are given in Tables 1 to 4.

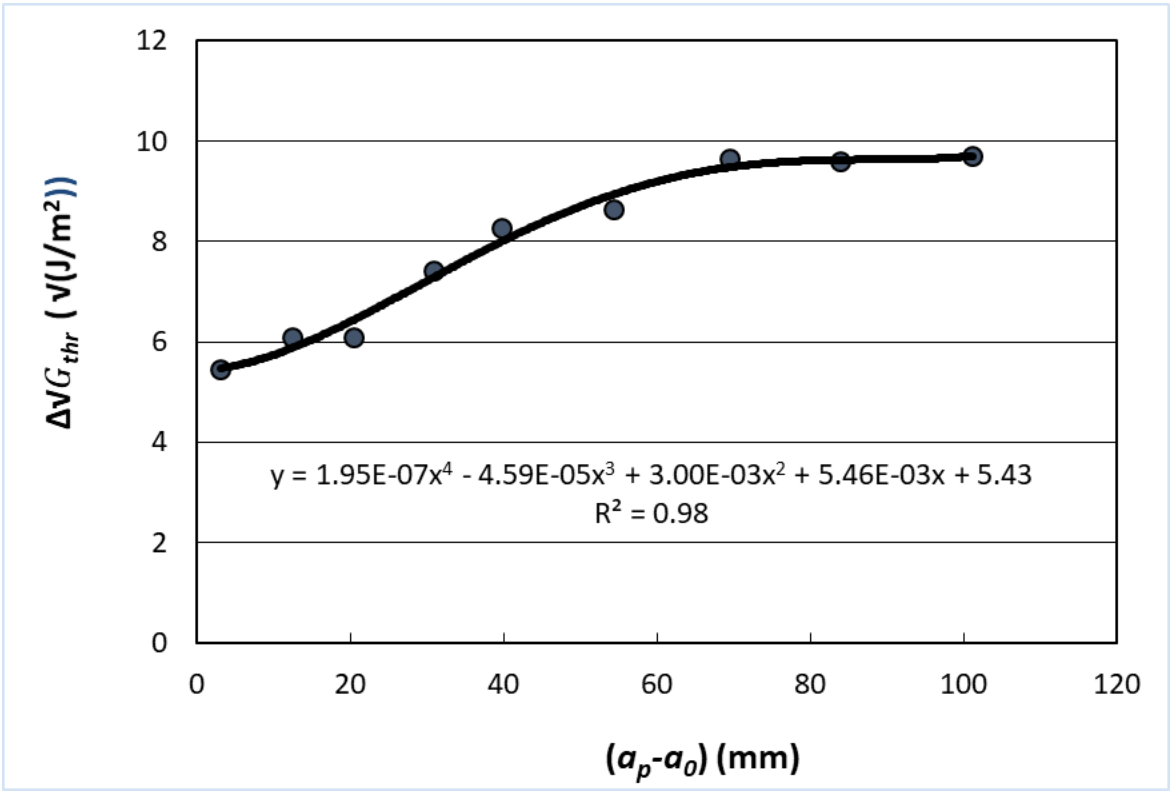
12
10
8
6
4
2
0
0
20
40
60
80
100
120
$\Delta v G_{thr}$ (v(J/m²))
y = 1.95E-07x⁴ - 4.59E-05x³ + 3.00E-03x² + 5.46E-03x + 5.43
R² = 0.98
$(a_p\text{-}a_0)$ (mm)

(a)

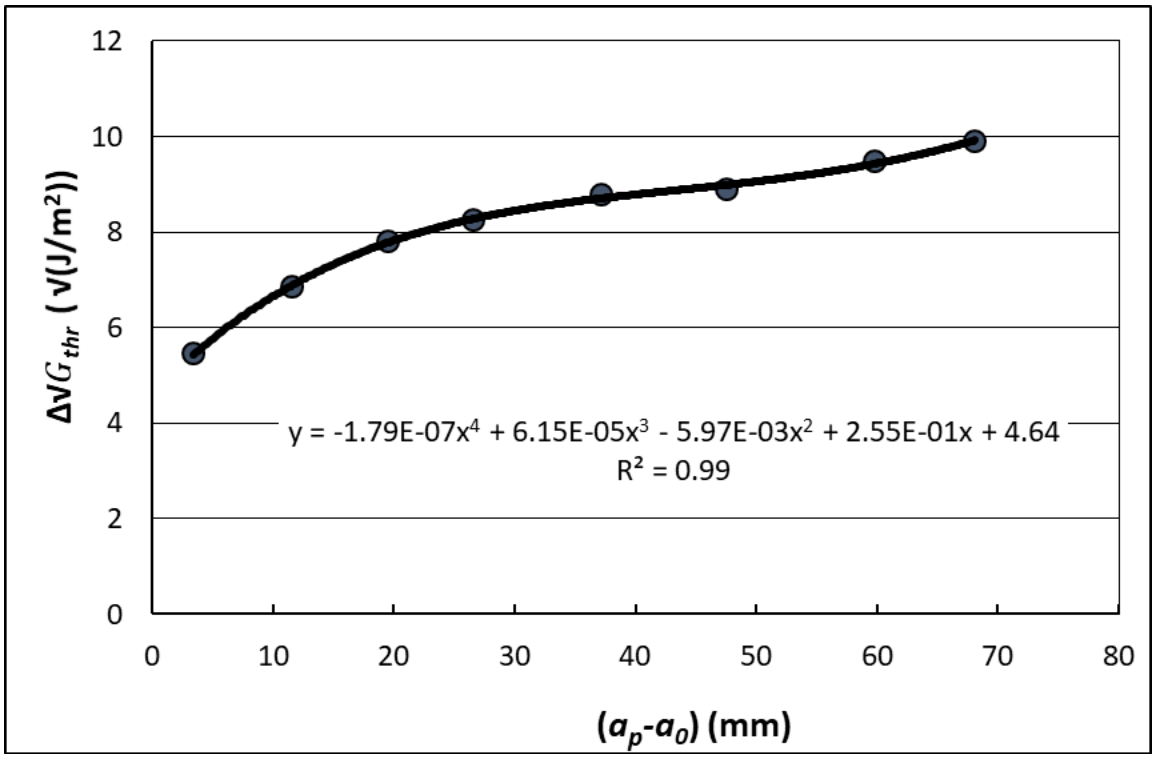
12
10
8
6
4
2
0
0
10
20
30
40
50
60
70
80
$\Delta v G_{thr}$ (v(J/m²))
y = -1.79E-07x⁴ + 6.15E-05x³ - 5.97E-03x² + 2.55E-01x + 4.64
R² = 0.99
$(a_p\text{-}a_0)$ (mm)

(b)

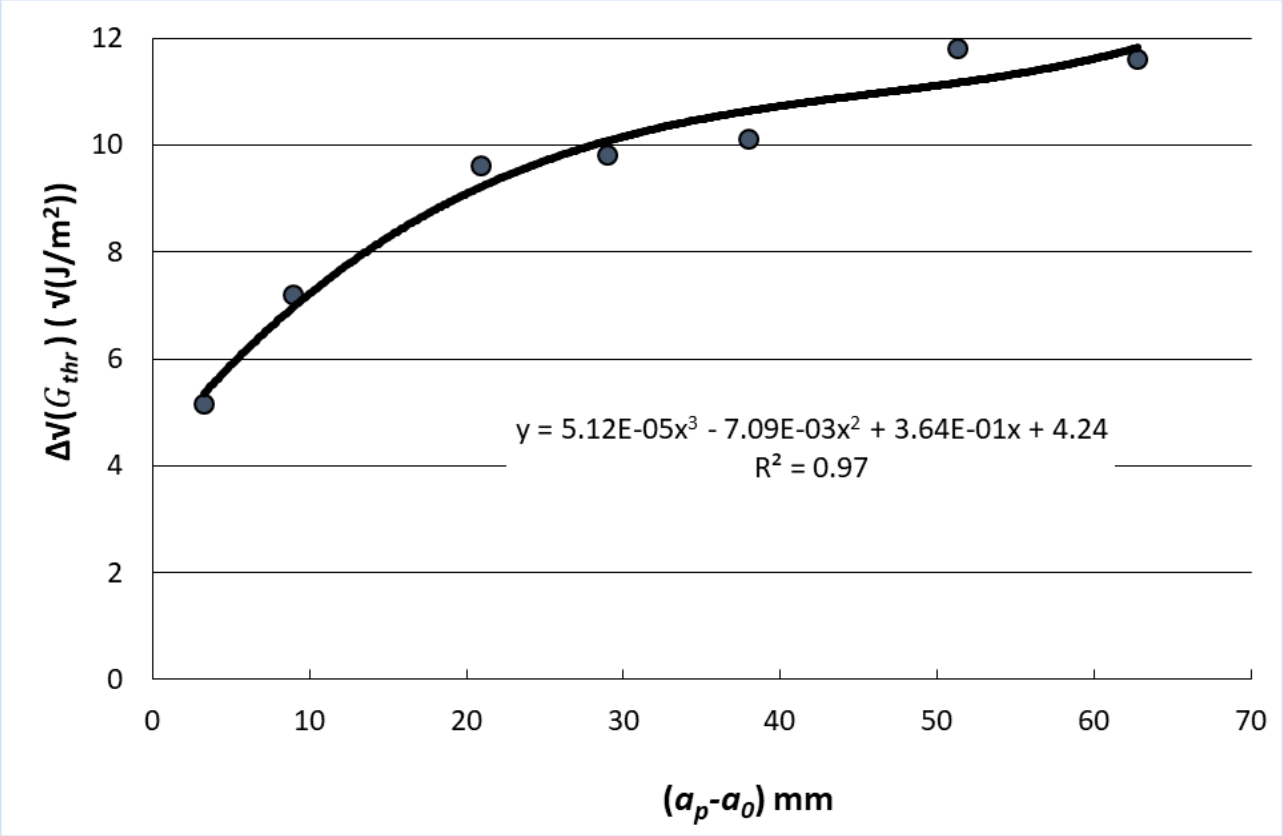

(c)

Figure 9. The $\Delta\sqrt{G_{thr}}$ versus (a_p-a_0) curves for three different test programs, with the data taken from Tables 1 to 4 as appropriate. For: (a) the unidirectional 48 ply composite tested at an *R*-ratio of 0.5, as shown in Figure 3, (b) the unidirectional 32 ply composite tested at an *R*-ratio of 0.5, as shown in Figure 1, and (c) the multidirectional $(\pm 45/0_{12}/\overline{\mp}45)//(\pm 45/0_{12}/\overline{\mp}45)]$ composite tested at an *R*-ratio of 0.5, as shown in Figure 6.

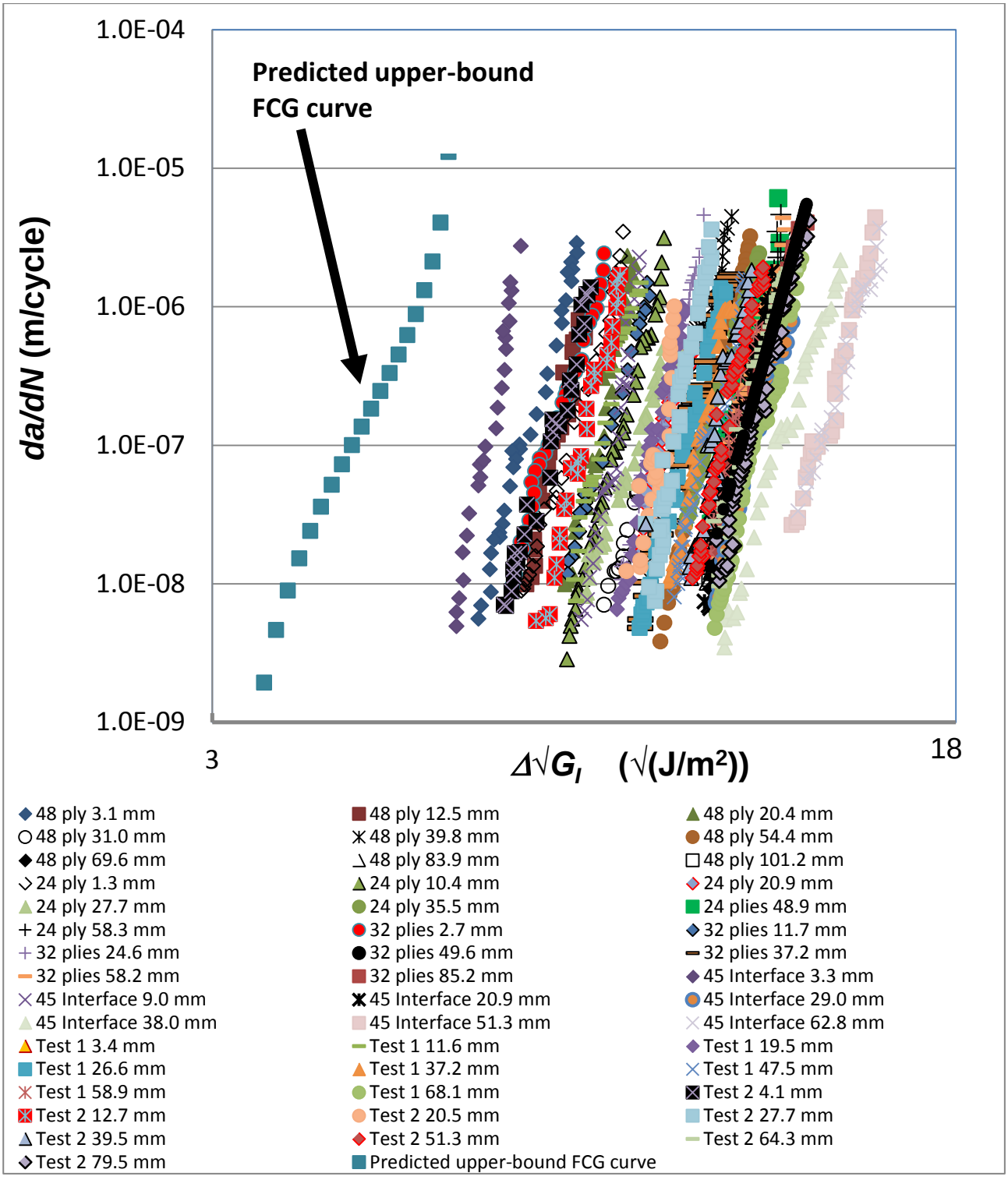

Figure 10. Experimental values of logarithmic *da/dN* versus logarithmic $\Delta\sqrt{G_I}$ from the laboratory test data, as shown plotted in Figures 1 to 6. Also given is the predicted 'upper-bound' FCG curve from Equation (3), using the values of $\sqrt{G_{thr0}}$ and G_{c0} (=A_0) based upon their respective mean values with minus three standard deviations, see Table 7.